Abschlussbericht DFG-Re 2653/1-2

1 Allgemeine Angaben

1.1	DFG-Geschäftszeichen	RE 2653/1-2
1.2	Antragsteller	Dr. Daniel Renusch Prof. Dr.-Ing. Michael Schütze (Da Herr Dr. Renusch zum 31.12.2008 aus der DECHEMA ausgeschieden ist wurde die Verantwortlichkeit für die Restlaufzeit auf Prof. M. Schütze übertragen)
1.3	Institut/Lehrstuhl	Karl-Winnacker-Institut der DECHEMA e.V. Theodor-Heuss-Allee 25 D-60486 Frankfurt am Main
1.4	Aus DFG-Mitteln bezahlte wissenschaftliche Mitarbeiter/ innen mit Angabe des Beschäftigungszeitraums	Dr. M. Rudolphi 01.02.2007 - 31.01.2009
1.5	Thema des Projekts	The Role that Hydrogen and Sulfur Play in Desktop Failure of Thermal Barrier Coatings
1.6	Berichtszeitraum Förderzeitraum insgesamt	01.02.2007 - 31.07.2009 01.02.2007 - 31.07.2009
1.7	Fachgebiet, Arbeitsrichtung	Werkstoffwissenschaften, Hochtemperaturkorrosion
1.8	Anwendungsfelder	Stationäre Gasturbinen, Flugtriebwerke, Dieselmotoren
1.9	Am Projekt beteiligte Kooperationspartner	Begleitung der Arbeiten durch J. L. Smialek vom NASA Glenn Research Center, Cleveland, OH, USA; Siemens Powergen, Mülheim; Alstom, Baden/CH; Rolls Royce Deutschland, Dahlewitz; MTU München.

Anm: Der Bericht ist in Englisch abgefasst, da der Antragsteller Herr Dr. Renusch US-amerikanischer Staatsbürger ist und eine enge Kooperation mit Dr. Smialek vom NASA Glenn Research Centre (Cleveland, OH, USA) für dieses Projekt bestand.

2 Zusammenfassung

2.1 Darstellung der wesentlichen Ergebnisse (Summary of the Results)

Thermal barrier coating systems usually fail immediately upon cooling from high temperature when the stresses generated by mismatch of the coefficients of thermal expansion (CTE) between the metallic bond coating and the thermally grown oxide layer (TGO) exceed a critical value. However, sometimes a special type of failure is observed, which is the failure of the TBC with a delay of minutes, hours, days or even weeks *after* the sample is at room temperature. This effect was named Desk Top Spallation (DTS) or Delayed Spallation (DS) since it was usually observed while samples were sitting on the desk top, waiting for further inspection [1].
The mechanisms involved in this special type of failure have been a mystery to research and industry for some time. One hypothesis brought up is that humidity from the office environment could play a role [2]. Also, sulfur from the substrate material was described as a potential contributor to failure, possibly in combination with water species [3-7]. Part I of this project started to provide some insight into the failure mechanism, nevertheless some questions remained unanswered and this follow-up project was started to further clarify the details of failure.

In part II of this project, which is covered in this report, new insight into the mechanism was gained and a deeper understanding of the processes taking place was developed. Over 100 specimens were tested under various conditions. Specimens were oxidized in four different atmospheres: (i) synthetic dry air, (ii) synthetic air & 10 vol.% H_2O, (iii) synthetic air & 50 vol.% H_2O and (iv) synthetic air & 10 vol.% H_2O & 0.1 vol.% SO_2. Some additional oxidation tests were carried out in laboratory air. Details about the specimens and testing procedures can be found in section 3.2.

Undoubtedly, desk top spallation is a very complex failure mechanism. The experiments have provided us with new information to conclude the major facts in this concealed damaging mechanism:

Water species (i.e. gaseous or liquid water) present around the thermally grown oxide layer and high intrinsic stresses in between the bond coat and the ceramic top layer after preceding oxidation do play the major role in desk top spallation.

While the application of liquid water or water vapor to oxidized specimens can cause noticeable moisture induced damage (i.e. increased acoustic emission, micro-cracking, and finally macro-cracking and spallation), there is no significant effect of moisture on as sprayed specimens or specimens which experienced only very short oxidation times.

Highly sophisticated hydrogen analysis techniques, namely Particle Induced Gamma Emission (PIGE) and Nuclear Reaction Analysis – Proton Transmission (NRA-PT), were employed to investigate the role of hydrogen or water species in this special failure mechanism. The hydrogen measurements show that oxidation in humid environment results in hydrogen uptake into the TBC top layer. The hydrogen is almost evenly distributed in the YSZ and TGO, neither one of the used techniques for hydrogen analysis showed an additional increase of hydrogen at the bond coat/TGO interface.
Standard metallographic investigations show increased inward growing oxide in humid environments forming cauliflower-like features as reported in part I [8;9]. Oxide thickness and structure seem comparable for samples oxidized in 10 vol.% H_2O and 50 vol.% H_2O.

The most important findings and conclusions about the complex mechanism of delayed spallation can be summarized as follows:

- Hydrogen is evenly distributed in the YSZ and TGO. Both hydrogen analysis techniques show that hydrogen is present in the YSZ and TGO. Much less hydrogen is found in the bond coat material.
- Literature provides several mechanisms that could potentially be involved in the DTS mechanism:
  - (i) Water and hydrogen could lower the binding strength in alumina and cause lower critical stress levels for cracking and higher crack growth rates [10-12]
    $\mathbf{Al_2O_3 + H_2O \rightarrow \sigma_c \downarrow}$
  - (ii) Water could react with the aluminum from the bond coat and form either gaseous hydrogen [13] or hydrogen ions [14]
    $\mathbf{Al_{alloy} + 3H_2O \rightarrow Al(OH)_3 + 3/2H_2 \uparrow}$ **or** $\mathbf{Al_{alloy} + 3H_2O \rightarrow Al(OH)_3 + 3H^+ + 3e^-}$
    This released hydrogen could then interact with the alumina according to (i)
  - (iii) Water could lead to a phase transformation of the tetragonally stabilized YSZ into the monoclinic phase, with resulting micro- and macro-cracking [15]
    $\mathbf{t\text{-}YSZ + H_2O \rightarrow m\text{-}YSZ}$
  - (iv) Sulfur from the substrate or the gas environment could reduce the interfacial strength at the TGO/bond coat interface [3-7]
- DTS is only observed after significant oxidation of the TBC system and the failure locus is the thermally grown oxide (TGO) layer. This indicates that the TGO layer is in the focus of the detrimental mechanism of desk top spallation.
- No significant detrimental effect of water on the YSZ layer was observed. The results from the 4 point bend testing, which are mainly influenced by the YSZ strength, show similar critical strain values for through TBC cracking after oxidation in dry and humid environment. Also, only very small amounts of monoclinic YSZ were found by XRD, no significant phase transformation from the tetragonal to the monoclinic phase is taking place.
- H_2O at high temperatures results in increased micro-crack formation in Al_2O_3 (TGO). The acoustic emission measurements show higher levels of acoustic emission when water is present in the oxidizing atmosphere. This micro-crack formation will lead to stress dissipation in the micro-crack network and a higher compliance of the TGO. For the APS system, this seems to reduce the failure probability during or after cooling.
- H_2O at temperatures slightly above room temperature results in increased micro-crack formation in the TGO. Delayed spallation was observed for both APS and EB-PVD coating types when pre-oxidation was sufficient to reach critical residual stress levels.
- Even small amounts of H_2O present at room temperature may help with crack initiation in the TGO. Even short exposures to ambient environment (e.g. removing the sample from the furnace and placing in an exsiccator) seem to be sufficient to allow enough water to enter the TBC system and cause delayed spallation.
- The TBC microstructure has a significant influence on the delayed spallation behavior. The EB-PVD system was found to be more vulnerable to DTS than both APS systems investigated. This is believed to be caused by the different microstructures of EB-PVD and APS coatings. Inward diffusion of water into the YSZ is possibly faster along the intercolumnar grain boundaries of EB-PVD coatings and slower in the interlocked splat

morphology of APS coatings. Also the considerably smoother TGO/bond coat interface of EB-PVD coatings provides a flat template for crack growth in and along the TGO, whereas in the rougher APS system, the crack would have to follow a complex geometry and might get stopped by running into the bond coat. Furthermore, the APS structure seems to have a higher compliance to compressive stresses due to the interlocking splats, which leads to higher critical strain values. Finally, differences in microstructure resulting from manufacturing can lead to different incubation times from specimen to specimen but also to different vulnerability for delayed spallation from batch to batch.

- SO_2 (g) in the oxidation environment evidently did not show a significant influence on delayed spallation behavior in the present investigations. No increased levels of sulfur were found around the TGO layer with Secondary Neutrals Mass Spectrometry (SNMS) after oxidation in SO_2 environment and no delayed spallation was observed.

2.2 Ausblick (Outlook)

With the new knowledge gained about the delayed spallation mechanism, the question remains what countermeasures can be taken to avoid moisture induced failure. Obviously, removing water vapor from turbines is not possible. Quite the contrary, thermal barrier coatings are recently incorporated in steam turbines where the H_2O content is at 100 vol.%. A second countermeasure could be to avoid unnecessary shut-downs of turbines to minimize micro-crack formation due to the CTE mismatch of metal substrate and ceramic top layer. Lifetime prediction modeling can help in determining the maximum operation durations, and current modeling approaches need to be further refined. Also, further development of thermal barrier coating systems with respect to new coating types and different microstructures can be beneficial in avoiding delayed spallation.

3 Arbeits- und Ergebnisbericht

3.1 Ausgangslage und Arbeitshypothesen (State of the Art and Working Hypothesis)

Failure of thermal barrier coatings if it takes place usually occurs immediately upon cooling after thermal treatment. This is mainly due to the mismatch of the coefficients of thermal expansion between metal substrate (i.e. bond coat) and the ceramic top layer (i.e. thermally grown oxide and YSZ top coat). Under certain circumstances, however, failure is observed with a delay of minutes, hours or even days after the sample is at room temperature (RT). This failure mode is called desk top spallation (DTS) since it was noticed when specimens were removed from the furnace and placed on the desk waiting for further inspection. Because this spallation occurs in ambient air, one working hypothesis was that water from the office environment could play a role. Frequently, water vapor related failure mechanisms in high temperature systems also involve sulfur, where for example sulfur can potentially react with H_2O at elevated temperatures to form sulfuric acid, which might lower oxide scale adhesion at the interface. The presence of sulfuric acid, even in dilute quantities, in the vicinity of the thermally grown oxide (TGO) is very likely to cause a drop in the interfacial adhesive strength and in turn produce an accelerated degradation process.

In order to evaluate the above hypothesis the quantification of the amount of hydrogen at the buried interface in the vicinity of the thermally grown oxide (TGO) is of critical importance. The detection and measurement of hydrogen on the ppm level is not possible with standard measurement technique, such as, x-ray diffraction (XRD), energy dispersive x-ray (EDX), and electron probe microanalysis (EPMA). A new approach using nuclear techniques for hydrogen analysis was developed in the framework of part I of this project, however, only few results have been produced during part I [8].

In part I of the project the specimens were oxidized isothermally at 1100°C in primarily the following atmospheres.

1. Synthetic air
2. Synthetic air plus H_2O (2.5% by volume)
3. Synthetic air plus SO_2 (0.01% by volume)

However, the hydrogen analyses performed on specimens exposed in those atmospheres showed no significant increase in hydrogen levels at the interface region between bond coat and thermally grown oxide, where failure is usually located [8]. Also, no traces of sulfur could be found at the same interface with SNMS measurements [8]. Hence, the water vapor content in the oxidizing atmosphere was increased to 10 vol.% and 50 vol.% for the experiments conducted in part II, to provide a higher possibility for inward diffusion of H_2O and potential crack formation. Similarly, the SO_2 content was increased to 0.1 vol.% with the same intention.

3.2 Beschreibung der durchgeführten Arbeiten (Description of the Work Performed)

3.2.1 Samples

The sample substrates of the systems investigated in this study were made from Ni-based superalloy (CM 247 and Haynes 214). The bond coats were 150 µm thick vacuum plasma spray (VPS) MCrAlY. The ceramic top coats were atmospheric plasma spray (APS) Zirconia coatings stabilized with 7 wt.% Yttria (7YSZ) of 300 µm thickness and with ~12% cumulative porosity. These samples were produced at the Forschungszentrum Jülich by Dr. Vaßen and Dr. Rauwald.

Two APS spray batches were used during this project, namely APS(1) and APS(2), where the second batch APS(2) was produced after a major revision of the VPS facilities at the FZ Jülich. The coating stability (i.e. lifetime) of APS(2) samples was higher than for APS(1) samples, no spallation was observed for isothermal oxidation times of up to 1500 h at 1100°C in humid or dry environment, while for the APS(1) samples the lifetime at 1100°C was typically around 1000 h. Furthermore EB-PVD YSZ coatings of 300 µm thickness have also been used. The EB-PVD samples were produced by Dr. Schulz at the Deutsches Zentrum für Luft und Raumfahrt (DLR) in Köln/Portz. Again, CM 247 Ni based superalloy was used as substrate

The sample geometries were: Oxidation cylinders (∅ 10 mm x 30 mm), Oxidation coupons (30 mm x 30 mm x 4 mm) and 4 pt. bend samples (80 mm x 6 mm x 4 mm).

3.2.2 Oxidation Environment

The testing environments utilized in this project were:

1. synthetic air (reference atmosphere, dry)
2. Synthetic air plus H_2O (10 vol.%)
3. Synthetic air plus H_2O (50 vol.%)
4. Synthetic air plus SO_2 (0.1 vol.%)

Testing has primarily been conducted isothermally at 1100 °C, additional isothermal exposures have also been made in laboratory air.

Cooling to room temperature was achieved in two ways: 1) rapid quenching to room temperature from 1100 °C or 2) furnace cooling to 800 °C, holding at 800 °C for at least 1 hr followed by rapid quenching to room temperature. During quenching the samples cool to room temperature in about 15 minutes.

Tables 1 and 2 summarize the exposure conditions for the isothermal exposures conducted in the framework of part II of this project. Additional exposures were carried out in laboratory air for post-oxidation acoustic emission measurement in liquid water and in humid vs. dry atmosphere.

Table 1: Isothermal exposures of APS coated samples at 1100°C

Environment	**200 hr**	**400 hr**	**670 hr**	**800 hr**	**1200 hr**	**1500 hr**
Synthetic air	2 coupons 2 4pt. bend	-	2 coupons 2 4pt. bend	2 coupons 2 4pt. bend	2 coupons 2 4pt. bend	2 coupons 2 4pt. bend
Synthetic air plus 10% H_2O	2 coupons 2 4pt. bend	-	2 coupons 2 4pt. bend	2 coupons 2 4pt. bend	2 coupons 2 4pt. bend	2 coupons 2 4pt. bend
Synthetic air plus 50% H_2O	2 coupons 2 4pt. bend	-	2 coupons 2 4pt. bend	2 coupons 2 4pt. bend	2 coupons 2 4pt. bend	2 coupons 2 4pt. bend
Synthetic air plus 10% H_2O plus 0.1% SO_2	1 coupons 1 4pt. bend	1 coupon 1 4pt. bend	-	1 coupons 1 4pt. bend	1 coupons 1 4pt. bend	-

Table 2: Isothermal exposures of EB-PVD coated samples at 1100°C

Environment	200 hr	250 hr
Synthetic air	1 coupon 2 4pt. bend	1 coupon 2 4pt. bend
Synthetic air plus 10% H_2O	1 coupon 2 4pt. bend	1 coupon 2 4pt. bend
Synthetic air plus 50% H_2O	1 coupon 2 4pt. bend	1 coupon 2 4pt. bend

3.2.3 Testing and Post-test Characterization

Acoustic Emission Measurement

Crack initiation and crack growth processes involve the generation of sound waves that can be detected in-situ with the acoustic emission method. This technique was therefore utilized to detect cracking within the specimens in various experiments, for example during high temperature oxidation, but also as a post-oxidation observation method. This technique proved especially useful since desk top failure is a delayed process and the failure time cannot be predicted. The AE measurements were carried out using MISTRAS PC interface cards (Physical Acoustics Inc.) in conjunction with two wide range (100 -1000kHz) sensors to enable location filtering of the recorded sound events.

Hydrogen Detection

One of the main objectives of this project was to detect hydrogen in the vicinity of the TGO layer in order to determine, whether hydrogen is accumulated in the depth region where failure occurs. Two methods have been used to follow this aim:

A) Detection using Particle Induced Gamma Emission (PIGE) and the Spallation Device for Ion Beam Application (SDIBA)

A specially designed vacuum chamber was built during part I of this project that includes a 4-point bending mechanism into a vacuum chamber for nuclear reaction analysis [8].

The ~300µm thick YSZ top layer is removed by forced spallation under vacuum to grant access to the buried TBC/TGO interface region due to the limited depth range <1µm that can be analyzed with the PIGE technique. Removing the TBC under vacuum is to avoid contaminations of the newly formed delamination surface with water from the laboratory environment. Additional hydrogen measurements were carried out to investigate the hydrogen content of the YSZ top layer before spallation.

These measurements were carried out at the Dynamitron Tandem Laboratory of the Ruhr Universität Bochum with the help of Dr. Meijer and Dr. Becker.

B) Detection using Nuclear Reaction Analysis Proton Transmission (NRA-PT)

This nondestructive technique for hydrogen analysis involves a high energy proton microbeam. The sample has to be thinned to below 100µm so that the proton beam can transmit through the specimen. Hydrogen in the sample is identified by coincidence proton-proton scattering under a scattering angle of 90°. Energy dispersive and space-resolved detection of the two emitted protons enables the calculation of the initial hydrogen position in 3 dimensions. By this way hydrogen mappings as well as depth profiles can be calculated from the raw data.

These hydrogen measurements were performed by Dr. Reichart at the Maier-Leibnitz-Laboratorium der Universität München und der Technischen Universität München.

Sulfur Detection by Secondary Neutral Mass Spectrometry (SNMS)
Secondary Neutral Mass Spectrometry is a destructive technique for elemental analysis. Argon ions are extracted from a plasma and accelerated towards the specimen. When the Ar-ions collide with the specimen they atomize (sputter) the specimen and generate neutral atoms of the constituent species. These neutral atoms are afterwards ionized and mass-analyzed. The depth resolution of this technique is in the nm range and detection limits usually are in the ppm range. However, sulfur is difficult to detect at low levels due to a superposition with signals from $^{16}O_2^+$-ions which have identical mass/charge ratio and cannot be separated from the $^{32}S^+$-ions. Therefore the signals from $^{34}S^+$ were also collected.

Critical Strain Measurements
The mechanical properties of the specimens were investigated with a conventional four point bend test that also uses acoustic emission to detect micro cracking processes within the TBC system. The test apparatus is described in more detail in references [16;17]. One prominent information that can be extracted from the measurement is the critical strain at which failure of the coating occurs. This value is dependent on sample pre-oxidation and ageing conditions.

Post Experimental Metallographic Investigation
Standard metallographic investigations were carried out to analyze the TGO growth kinetics. These include the preparation of cross-sections of the pre-oxidized coupon samples and inspection and analysis under the optical microscope. In some cases Scanning Electron Microscopy (SEM) was used for additional phase investigations.

X-Ray Diffraction (XRD)
X-Ray Diffraction measurements allow a phase analysis of (poly-) crystalline materials. A SIEMENS D 500 MP diffractometer available at the Karl-Winnacker Institute was used for identification of the phases in the YSZ top coating before and after oxidation.

3.3 Darstellung der erzielten Ergebnisse (Results)

The results of the DFG project “The Role That Hydrogen and Sulfur Play in Desk Top Failure of Thermal Barrier Coatings” (RE 2653/1-2) show that both water vapor and liquid water in combination with pre-oxidation and high stresses in the TBC system can trigger delayed spallation.

3.3.1 Desktop Failure Map
The most important observations about the occurrence of Desk Top Spallation (DTS) made during this project are summarized in a “Desktop Failure Map”, figure 1. It gives an overview about conditions that can lead to DTS. The different oxidation conditions and the outcome with respect to delayed spallation (i.e. DTS was observed or not) are listed for the three different TBC systems investigated.
EB-PVD coatings showed Desk Top Spallation in almost every condition used in this project and had a spallation lifetime of around 200 hours. Note, EB-PVD coatings usually exhibit longer lifetimes under thermal cyclic loading conditions. However, cyclic testing in humid environments is a difficult task, since condensation of water on the specimen has to be avoided. Hence, no cyclic oxidation tests were carried out during this project.

We will go through the different testing conditions and the observed outcome quickly and the detailed discussion will be covered in separate sections later on:

Condition (1): isothermal oxidation in laboratory air at 1100°C and succeeding liquid water application (water immersion or water dripping) at room temperature. The pre-oxidized EB-PVD samples showed DTS in the water drop experiment (details see section 3.3.4, figure 6) while the APS(1) samples did not show macroscopic cracking in water immersion experiments (section 3.3.5, figs. 8 & 9). This difference is believed to be caused mainly by the different microstructure of APS and EB-PVD systems. The columnar structure of the EB-PVD allows easier access for the water to the TGO whereas the splat morphology of APS samples leads to slower penetration along the zigzagging splat boundaries.

Condition (2): isothermal oxidation in laboratory air at 1100°C and succeeding water vapor exposure at ~50°C. DTS was observed for both APS and EB-PVD coatings (see section 3.3.6, figures 11 & 13). Probably the permeation of water vapor at temperatures slightly above RT is faster than that of liquid water at RT leading to spallation in both coating types.

Condition (3): isothermal oxidation in laboratory air at 1100°C and succeeding storage in dry air (i.e. in an exsiccator) at room temperature. Under this condition no DTS was observed on the APS(1) sample (section 3.3.6, figure 12) since no sufficient amount water vapor was present during the post-oxidation storage. However, delayed spallation was observed on the EB-PVD coated sample (section 3.3.6, figure 10), probably due to very small amounts of water vapor from the laboratory environment that had entered the TBC structure between removal from the furnace and placement in the dry air container. Furthermore, the columnar structure of the EB-PVD YSZ is more brittle than the splat structure of APS coatings, where the overlapping and interlocked splats form a more sturdy top coating.

Condition (4): isothermal oxidation in dry synthetic air at 1100°C and succeeding storage in laboratory air. This condition resembles the usual way that researchers perform their oxidation testing and is hence the condition under which DTS is mostly observed. In our study DTS was observed for APS(1) and EB-PVD samples. No DTS was observed for APS(2) samples. The structural stability and isothermal lifetime of the APS(2) batch was obviously much higher than those of the APS(1) samples. The strain energy in the system accumulated after 1500h oxidation was still too small for stable crack growth and spallation to occur. For the APS(1) samples with lower structural strength the availability of a small amount of water from the laboratory air evidently is sufficient to cause stable microcrack growth and DTS. Note, the APS(1) samples were stable in the dry air environment (condition (3)). The EB-PVD samples, which need considerably lower water vapor levels (compare condition (3)) to show DTS, consequently spall also under this condition.

Conditions (5 & 6): isothermal oxidation tests at 1100°C in synthetic air plus 10 vol.% H_2O and synthetic air plus 50 vol.% H_2O, respectively, followed by storage in laboratory air. Again, desk top spallation was observed for the EB-PVD samples, however, both the APS(1) and the APS(2) samples remained intact. The tougher structure of APS coatings in conjunction with water present at high temperatures leads to stress relief in the TBC structure by microcrack formation, which was detected with acoustic emission monitoring during oxidation (see section 3.3.7, figure 14).

Condition (7): isothermal oxidation at 1100°C in synthetic air plus 10 vol.% H_2O plus 0.1 vol% SO_2 and succeeding storage in laboratory air. No desk top spallation was observed on the APS(2) samples that were oxidized for up to 800 hours. For APS(2), there seems to be no detrimental effect of SO_2 in the oxidizing environment on the spallation behavior of thermal barrier coatings compared to condition (5).

3.3.2 Hydrogen Detection using the Spallation Device for Ion Beam Application (SDIBA)

Hydrogen detection was one of the main aspects of this project and consequently a large number of samples were prepared for hydrogen analysis in the SDIBA chamber. The APS(2) samples chosen for this technique were oxidized in dry and humid atmospheres, respectively, at 1100 °C for durations of up to 1500 h. The intention of using humid atmosphere as oxidation environment was to charge the TBC with water or hydrogen species and to investigate a possible accumulation of hydrogen at the interface region between ceramic top coating and metallic bond coating.

The hydrogen content of the TBC top surface of the specimens oxidized at 1100 °C in different environments is given in figure 2. The strong peak at the surface is a superposition of hydrogen or water adsorbed at the surface and hydrogen embedded in the upper region of the specimens (the hydrogen content that is aimed at with this analysis). As can be seen from figure 2, for oxidation times of up to 200h no substantial inward diffusion of hydrogen takes place, however, after longer oxidation periods in humid atmosphere an increased hydrogen content can be found in the surface region of the YSZ top layer. This indicates that hydrogen species (i.e. H_2O, OH^- or H^+) enter the TBC through the porous ceramic top layer by inward diffusion processes.

Hydrogen depth profiles of the interface region TGO / bond coat are shown in figure 3. Here, the YSZ top layer was removed by 4-pt. bending under vacuum using the built-in mechanical device. However, it turned out that even exposing the interface region under vacuum could not prevent a surface contamination with carbohydrates from the residual gas in the vacuum chamber ($p_{chamber} < 5x10^{-6}$ mbar). Consequently the peaks shown in figure 3 are again a superposition of contamination and original hydrogen. It seems, however, that the surface hydrogen content of samples that were oxidized in humid atmosphere is slightly increased compared to the dry environment. If identical contamination levels are assumed, this could be an indication for an increased hydrogen level inside the crack network of those specimens oxidized in humid environment. If this hydrogen weakens the crack network, the delamination crack would most likely follow these hydrogen containing microcracks and as a consequence forced spallation would expose a hydrogen enriched surface.

3.3.3 Hydrogen detection using Nuclear Reaction Analysis Proton Transmission (NRA-PT)

The second analytical approach for hydrogen detection used in this project is a 3D mapping technique with µm resolution, that allows detection of hydrogen within a thin (<100µm) sample. Selected samples (again APS(2) samples) were prepared in cross-section and thinned by dry polishing with SiC paper to a thickness of about 80µm. Figure 4a shows an optical micrograph of the analyzed region taken with a microscope attached to the analysis chamber. The specimen shown here was oxidized for 800 h at 1100 °C in synthetic air & 10 vol.% H_2O. The region selected for analysis was chosen to cover the bond coat (left), the TGO layer (centre) and the YSZ top layer (right). Also given in figure 4 are two results of the computational analysis of the measurement data, where each dark point indicates a detected hydrogen event. Darker regions thus indicate higher hydrogen contents. Figure 4b is a hydrogen mapping and figure 4c a hydrogen depth profile. Three areas were marked in the hydrogen mapping (fig 4b) to match the bond coat (1), the TGO layer and interface region (2), and the YSZ top layer (3). The depth profile in fig. 4c represents the hydrogen content in z-direction (normal to the paper plane). The darker band at the top and the curved band at the bottom result from hydrogen species adsorbed at the specimen surfaces. The bottom band is curved due to proton energy loss in the 80µm thin cross-section which was not corrected for mathematically.

Figure 5 is a detailed analysis of the depth profile given in figure 4c and provides hydrogen mappings of different depth regions in the cross-section. The red and blue mappings were calculated from the surface regions and the green mapping is an approximation of the inner

volume of the specimen which was therefore not exposed to hydrogen species in laboratory air or the vacuum chamber. The green mapping is consequently not affected by contamination at all.
It can be seen that the hydrogen content in the YSZ is significantly higher when compared with the metallic bond coat material. Certain regions in the YSZ exhibit hydrogen accumulation, however, no significant accumulation at the TGO layer and the interface can be observed.

3.3.4 Video capture and Acoustic Emission of Moisture Induced Delayed Spallation

These tests were inspired by a video sequence from our NASA collaborators [18]. They captured probably the first video of water induced top coat failure, showing the complete spallation of the TBC within seconds after a few drops of liquid water were dripped onto the surface of a pre-oxidized EB-PVD TBC.
In order to reproduce this result a series of oxidation experiments with EB-PVD TBCs were designed which incorporated acoustic emission technique as well as video capturing to correlate the soundwaves from the cracking with visible spallation [19]. The sample was isothermally pre-oxidized at 1050 °C in laboratory air for 310 h, then removed from the furnace and quenched to room temperature within 5 minutes. Subsequently the acoustic emission equipment was connected and the subsiding of cracking due to thermal expansion mismatch stresses was monitored. After 30 minutes distilled water was dripped onto the cold TBC. Still images from the video clip and the correlation between acoustic emission and visible spallation are given in figure 6. A copy of the video clip is on the enclosed CD-ROM. As can be seen from figure 6, the acoustic emission increased immediately after the water was added, the TBC started to delaminate about 15 minutes afterwards. Complete delamination was achieved within about 15 seconds.
The acoustic emission of water dripping on an as-sprayed sample was determined with a sample that was dehydrated on a hot plate at approximately 120 °C for 90 min prior to connecting the AE sensors. Except for one random acoustic event, the sample remained silent before and immediately after the application of distilled water, proving that water itself is not generating sound waves as it is travelling through the channels of the columnar TBC structures. As expected, the as-sprayed, minimally damaged TBC did not spall.
Nevertheless, a slight increase in acoustic emission after water application was observed on a sample that was pre-oxidized for as little as 26 h at 1050 °C, as can be seen in the energy rate-diagram in figure 7a. Yet, the top coat did not delaminate due to an insufficient amount of stored strain energy in the TGO layer. This underlines the common understanding that a thermally grown oxide (TGO) layer and the intrinsic stresses from its growth are essential for cracking to occur. The failure locus of the delaminated sample (310 h at 1050 °C) was investigated with an SEM, two micrographs are exemplarily given in figure 7b and 7c. Fig. 7b shows the bottom side and a fracture edge of the YSZ top coat and fig. 7c is the revealed surface of the bond coat on the substrate. Remaining pieces of alumina on both sides clearly illustrate that the failure locus was around the TGO layer, with the crack running along the upper and lower interface of the TGO and through the TGO itself as well.

3.3.5 Water Immersion with Acoustic Emission

Another test involving liquid water was performed on an APS(1) sample that was pre-oxidized at 1100 °C for 1000 h in laboratory air and quenched to room temperature afterwards. The sample was attached to the acoustic emission setup and immersed into distilled water at room temperature. Images of the test setup and the immersed sample are shown in figure 8.
The acoustic emission of the sample was monitored for ~ 100 h in laboratory air before the sample was lowered into the water-filled beaker. Only a few acoustic events occurred during this period of time, but on contact with water the acoustic emission increased significantly (see figure

8a). The sample remained submersed for about 700 h and the acoustic emission continued at an increased level for the length of the immersion; however, the sample did neither spall nor show any visible cracks in the TBC. Upon removing of the sample from the water beaker the acoustic emission subsided and reduced to an amount similar to the noise recorded prior to the water immersion. Unfortunately, the uncoated part of the sample was also immersed in water during the test leaving the possibility that the recorded sound waves might have originated from the exposed oxide scale. Consequently a second experiment was conducted to investigate this possibility. Another cylindrical sample from the same batch APS(1) was chosen and was cut on both ends. The sample was pre-oxidized for 1000 h at 1100°C in synthetic air. Subsequently, the ends of the sample were ground with SiC paper to remove the oxide scale that was formed during oxidation and the sample was attached to the acoustic emission system and immersed in water as the other sample. A photograph of the sample and the acoustic emission signal recorded is shown in figure 9. Only very little acoustic emission was recorded over the observation time of about 900 hours. This indicates that the acoustic emission on the first sample (cf. fig. 8) was mainly from the exposed oxide scale at the upper end of the sample. Furthermore, this could be an indication that water inward diffusion through the APS TBC is very slow and since water has only limited access to the TGO layer the mechanism of moisture induced spallation is prevented.

3.3.6 Post-Oxidation Monitoring in Dry vs. Humid Environment with Acoustic Emission

In an attempt to reproduce desk top spallation under defined conditions a series of experiments were carried out with EB-PVD as well as APS coated samples. The samples were pre-oxidized to near-failure (i.e. about 90% lifetime) and stored in hermetically sealed reactor crucibles which either contained molecular sieve pellets to create a dry environment, or which were placed on a heating plate at about 50°C with some water added to create a humid environment. Furthermore, the samples were connected to acoustic emission sensors to record sound waves generated by cracking in the sample. The whole procedure of removing from high temperature, cooling to room temperature, connecting the samples to the acoustic emission sensor waveguides and finally placing in the reactor crucibles took about 30 minutes.

A photograph of the EB-PVD sample stored in dry environment is given in figure 10 together with the acoustic signals; the corresponding sample in humid environment is displayed in figure 11. Both samples were oxidized in laboratory air at 1050°C for 190h and placed in the reactor crucibles about 30 minutes after they were removed from the furnace at high temperature. Surprisingly, both samples spalled over night as can be seen in the respective photographs. However, there is a slight difference in the way the top coating delaminated and fractured. The sample in the dry environment spalled into small pieces (visible on the bottom of the reactor crucible) whereas the sample in the humid environment delaminated as one YSZ piece. This indicates that the delamination and spallation process in the dry environment was not continuous and that the stored strain energy was just below the critical value for dry fracture. A small amount of residual water might have been in the porous structure (either from oxidation in laboratory air or from handling in laboratory air after oxidation) acting as a crack starter mechanism for subsequent unstable multiple crack growth.

In the humid environment on the contrary more water molecules were available. This lead to a more continuous and stable crack growth rate resulting in a gentler release of the stored energy; which in the end was responsible for the YSZ top coating to stay in one piece.

The APS coated specimens from batch APS(1) were of cylindrical shape and oxidized at 1100 °C for 910 h (i.e. 90% lifetime) in laboratory air. Again, the samples were connected to the AE sensors and placed in the reactor crucible after removal from high temperature within about 30 minutes. The acoustic emission signal and a photograph of each sample are given in figure 12 and figure 13 for the dry and humid environment respectively. The acoustic emission subsided significantly for both samples after about the first 30 minutes in the closed environment. An increase of acoustic emission is visible at the time where a few drops of water were added to the

heated crucible (cf. fig. 13), which corresponds to microcrack formation. After about 1.5 hours the acoustic emission of the sample in humid environment increased significantly and the macrocrack began to form. The sample stored in the dry environment on the other hand remained intact over the total monitoring duration of about 350 hours and showed much less acoustic emission.

3.3.7 Oxidation at 1100°C with Acoustic Emission Measurement

The amount of cracking that occurs at high temperatures was investigated in isothermal exposure experiments at 1100 °C in three different atmospheres, namely synthetic air, synthetic air & 10 vol.% H_2O and synthetic air & 50 vol.% H_2O. APS samples from batch APS(1) were chosen for this test. The acoustic emission data of the sample oxidized in dry synthetic air is given in figure 14a. During the whole hot dwell time of 1000 h only a few acoustic events were recorded. This indicates that there is no significant cracking in the sample when hot. The vast majority of acoustic emission is generated during cooling from 1100 °C to room temperature with the first events occurring at temperatures around 800 °C and the acoustic emission slowly diminishing over the following days. As can be seen in figure 14b the sample that was oxidized in dry synthetic air spalled upon cooling from high temperature, whereas the two samples oxidized in the humid environment both remained intact. The analysis of the acoustic emission from those two specimens (see figures 14c and 14d) reveals that a higher amount of micro-cracking occurs at oxidation temperature in the humid environments and that the energy release per acoustic event is also higher than in the dry environment. This high temperature micro-cracking will decrease the strain energy build-up in the TBC system and result in lower stored strain energy after cooling also. Consequently the stored strain energy was too small on those samples to cause spallation.

3.3.8 Critical Strain Measurements

The mechanical properties of the oxidized APS(2) specimens were investigated with 4 point bend testing at room temperature as a function of exposure time and environment. A typical example of the stress/strain curve and acoustic emission signals that are recorded during bending is given in figure 15. The drop in the stress/strain curve and the peak in the acoustic emission indicate where failure (i.e. through cracking) of the top coating occurs.

The critical strain values for through cracking obtained from the different samples are given as a function of exposure time and environment in figure 16. The specimens that were pre-oxidized in humid environment show a tendency towards slightly lower critical strain values, however, the values are more or less in the same range. Since the ctritical strain values for through cracking obtained by this test are mainly influenced by the YSZ top coating, this indicates that the oxidation in humid environments does not lead to a significant deterioration of the YSZ compared with oxidation in dry environment.

3.3.9 Sulfur Detection by Secondary Neutral Mass Spectrometry (SNMS)

The sulfur detection measurements carried out in part I of this project showed only small amounts (below 0.1 at.%) of sulfur in the vicinity of the TGO layer after oxidation in synthetic air & 0.01 vol.% SO_2 [8]. These measurements were conducted on samples that were used beforehand in the PIGE experiments, batch APS(2), where the TBC/TGO interface layer was exposed by forced spallation in the SDIBA chamber. As a consequence, the surface consisted of a mixture of remnants of YSZ, exposed TGO and to a small amount of exposed bond coating material. The reason why no sulfur was found in these experiments was believed to be either (i) an insufficient amount of SO_2 offered in the oxidation atmosphere; (ii) insufficient transport of sulfur species into the TBC system and hence no accumulation at the TBC/TGO interface; or (iii)

that the new surface created by the forced spallation of the TBC top layer was not as close to the TBC/TGO interface as intended.
The approach in part II of the project was therefore to drastically increase the available SO_2 in the oxidation environment by a factor of 10 to 0.1 vol.%; and to try another way to expose the TBC/TGO interface. The samples selected for analysis were laser-ablated using the Nd:YAG laser of the DECHEMA micro-manufacturing laboratory. The results of two samples oxidized at 1100 °C for 800 h in synthetic air vs. synth. air & 10vol.% H_2O & 0.1vol% SO_2 are given in figure 17. As can be seen, the signals for sulfur (either ^{32}S or ^{34}S) are not changing over the total depth range investigated and are at a very low intensity corresponding to concentrations of approximately around 0.05 at.%. No indications of an accumulation of sulfur was found, neither on the sulfur exposed nor on the synthetic air exposed sample. Obviously, no significant inward diffusion of SO_2 occurs through the APS YSZ top layer.

3.3.10 Discussion of Experimental Results and Proposed Mechanism

The presented results provide definite proof that water, be it in gaseous or liquid form, is detrimental for thermal barrier coatings that have undergone a thermal treatment. The magnitude of the effect is dependent on the pre-existing strain energy within the sample and also on the pre-existing micro-crack network. Hydrogen analysis has shown that hydrogen is almost evenly distributed in the YSZ top layer as well as in the TGO and that hydrogen uptake during oxidation in humid environment occurs. REM investigations have shown that the failure locus is around the thermally grown oxide layer, with cracks running along both the YSZ/TGO interface and the TGO/BC interface as well as through the TGO itself. It thus seems plausible that the main impact site for this moisture induced damaging mechanism is the alumina of the TGO layer.
Wiederhorn and Charles report increased crack growth rates in the presence of water vapor for glass and sapphire [11;12;20;21]. This would affect the TGO itself and the TGO/bond coat interface, possibly also the TGO/YSZ interface. Also, the generation of hydrogen by a reaction of aluminum powder with distilled water was observed [13] which could provide another source for hydrogen species at the TGO/bond coat interface. The released hydrogen could then enter the TGO and act according to Wiederhorn and Charles to increase crack growth rates. There is also the possibility of a degradation of the tetragonally stabilized YSZ by water which was described by Yoshimura [15]. Indeed small fractions of the monoclinic zirconia phase have been observed with XRD after oxidation in humid environment (cf. figure 18) however, since the crack path in DTS is usually along the TGO/bond coat or TGO/YSZ interface it seems more likely that the degradation of alumina is the major mechanism in DTS. Lawn provides an atomistic model of crack growth in alumina in which the strongly linking oxygen ions are replaced by weakly coupled hydroxyl pairs[10]:

$$(–Al–O–Al–) + (H–O–H) \rightarrow (–Al–O–H \; . \; H–O–Al–)$$

A graphical illustration of this mechanism is given in figure 19.

Concluding that energy required for crack opening is higher in a dry environment than in a humid environment (e.g. $G_{c,\,humid} < G_{c,dry}$) the transport of water into the crack tip is consequently of critical importance also. The crack will only grow as long as one of the following prerequisites is true:

- high local stresses at the crack tip (strain energy > $G_{c,\,dry}$) to provide enough energy for crack opening without the presence of water
- high local stresses at the crack tip (strain energy < $G_{c,\,dry}$) *and* access for water molecules to crack tip

The geometric condition of the TBC system is another very important factor in the failure mechanism. This becomes evident when looking at the differences between EB-PVD coatings and APS coatings and was mentioned in the discussion of the Desktop Failure Map in section 3.3.1. Figure 20 highlights the two major differences between EB-PVD and APS coatings and their impact on the DTS mechanism.
APS coatings exhibit a "splat morphology" which is caused by the molten droplets of YSZ solidifying shortly after impact on the substrate during deposition. These droplets are thicker in the centre and thinner to the sides and overlap in a random distribution. As a consequence the APS YSZ layer consists of interlocking splats and pathways for inward diffusion along the splat boundaries are very complex and considerably longer than the coating thickness. The EB-PVD type coatings on the other hand grow in a polycrystalline manner forming a columnar structure and exhibit gaps between the columns which enable easier inward diffusion along a straight line from surface to the YSZ/bond coat or YSZ/TGO interface. This indicates that inward diffusion of water is considerably faster in EB-PVD coatings. Furthermore, the splat morphology of APS coatings may yield a higher compliance (with regards to compressive stresses) of APS coatings after cooling compared with EB-PVD coatings. This reduces the intrinsic stress levels of APS coatings.
The other major difference in geometry between the two coating types is the interface morphology. The EB-PVD coatings are usually deposited onto a polished surface and consequently the interface between bond coat and YSZ is very flat. As the TGO layer forms at this interface, the shape does not change. The APS coatings are usually deposited onto a much rougher surface and as a consequence the bond coat/TGO interface is bent and of complex shape. A crack running along such an interface would have to follow this bent structure and might get stopped by running into the bond coat.
Both of these factors make the EB-PVD coatings more vulnerable towards moisture induced failure and give an indication why batch to batch deviations in lifetime are observed.

3.4 Ausblick auf zukünftige Arbeiten (Outlook for Future Research)

The negative effect of moisture on TBC stability and adhesion is an undeniable fact, as was clearly demonstrated by this work. The conclusions that can be drawn from this project indicate that not only TBC systems or alumina scales are vulnerable to moisture induced spallation, but possibly other oxides as well. For example SiO_2 is also known to have higher crack growth rates in the presence of water or water vapor [11;12;20;21]. Consequently we have started another research project to investigate the role of moisture on other metal oxides (i.e. oxide scales on metal) that are commonly used in high temperature applications. This fundamental study should further clarify the effect of H_2O on oxides.

3.5 Interdisziplinäre Weiterentwicklung

As a material science research project all of the results and publications are in a sense of interdisciplinary interest. High temperature oxidation is part of the field of solid state chemistry. Stresses, strains, critical strains and fracture are from engineering. Acoustic emission is part of the field of physics. Proton induced gamma-ray emission and nuclear reaction analysis proton transmission are part of the field of nuclear physics.
The use of highly sophisticated analysis techniques like PIGE, NRA-PT and SNMS, which were previously not well established in the engineering community and combination of interdisciplinary research has resulted in the development of a fundamental understanding of the mechanisms involved in desk top spallation. The DTS failure map given in figure 1 can be of high value to both researchers and industry.

3.6 Verwertungspotential

The results of this project have been presented to the representatives of several gas turbine manufacturers, namely, Siemens, Rolls-Royce, MTU, as well as to the Durability and Protective Coatings Branch of the NASA Glenn Research Center. All of these colleagues identify the results of this project as a significant contribution to understand TBC spallation and service life time. There is a strong interest in further developing the results and approaches produced by this project, especially the investigation of other metal oxides.
The Desktop Failure Map (figure 1) generated during this project will help as an approach to check the implications of oxidation and post-oxidation treatments on the vulnerability of thermal barrier coatings with respect to delayed failure. Also this project has shown that there is a difference between oxidation testing in laboratory air and oxidation testing in synthetic dry air, since there is an effect of water on the oxide growth and oxide stability. If highly reproducible results are required, oxidation testing in dry synthetic air is absolutely necessary.

3.7 Beteiligte Wissenschaftler

Dr. Renusch was the guiding scientist of the project. The research work of the project was performed by Dr. Rudolphi. Dr. Zschau provided technical assistance with the construction and operation of the SDIBA apparatus. Dr. J.L. Smialek from the NASA Glenn Research Centre, Cleveland, OH, USA was cost neutral project partner and helpful with many fruitful discussions. Dr. Meijer and Dr. Becker provided technical assistance with the beam line at the 4 MV Dynamitron-Tandem Accelerator of the Ruhr-Universität-Bochum. The NRA-PT measurements were carried out at the Tandem Accelerator of the Accelerator Laboratory of the Technische Universität München by Dr. Reichart**.** The secondary neutral mass spectrometry measurements were conducted by Dr. Sommer from the Forschungszentrum Karlsruhe. The VPS MCrAlY coating and APS top coats were sprayed by Mr. Rauwald and Dr. Vaßen of the Forschungszentrum Jülich. The EB-PVD coatings were produced by Dr. Schulz from the Deutsches Zentrum für Luft- und Raumfahrt (DLR) in Köln-Porz.
The help of all these colleagues is gratefully acknowledged.

4 Liste der Publikationen aus dem Projekt

The publications from part I of this project can be found in reference [8].

4.1 Published Journal Papers (The Full manuscripts are attached):

1. **Detection of Hydrogen in Hidden and Spalled Layers of Turbine Blade Coatings**, M. Rudolphi, D. Renusch, M. Schütze, J. Meijer
   Presented at the 36th International Conference on Metallurgical Coatings and Thin Films, April 27 – May 1 ,2009 (San Diego, CA, USA), will be published in special issue of Surface and Coatings Technology.
2. **The effect of moisture on the delayed spallation of thermal barrier coatings: VPS NiCoCrAlY bond coat & APS YSZ top coat**
   M. Rudolphi, D. Renusch, H.-E. Zschau and M. Schütze
   Materials at High Temperatures 26 (2009) 325–329
3. **Verification of moisture-induced delayed failure of thermal barrier coatings**, M. Rudolphi, D. Renusch and M. Schütze
   Scripta Materialia 59 (2008) 255–257
4. **Hydrogen Detection in Buried Layers of Thermal Barrier Coatings**
   M. Rudolphi, D. Renusch, H.-E. Zschau, M. Schütze
   Materials Science Forum 595-598 (2008) 177-184
5. **Mechanisms of the Desk Top Spallation Effect**
   M. Rudolphi, D. Renusch, M. Dietrich, M. Schütze
   Oxidation of Metals (in preparation)

4.2 Contributions to Conferences - Posters (poster in A4 attached):

1. **Delayed Spallation of Thermal Barrier Coatings**
   M. Rudolphi, D. Renusch, M. Dietrich, H.-E. Zschau, P. Gawenda, M. Schütze
   Gordon Conference on High Temperature Corrosion 2007, New London, NH, USA
2. **The role that hydrogen and sulfur play in desktop failure of thermal barrier coatings**
   M. Rudolphi, D. Renusch, H.-E. Zschau, M. Schütze
   15. Jahreskolloquium des Karl-Winnacker-Instituts der DECHEMA e.V., November 29, 2007, Frankfurt am Main, Germany.
3. **Hydrogen Detection in Buried Layers of Thermal Barrier Coatings**
   M. Rudolphi, D. Renusch, H.-E. Zschau, M. Schütze
   7th International Symposium on High Temperature Corrosion and Protection of Materials, May, 18-23, 2008, Les Embiez, France.
4. **The effect of moisture on the delayed spallation of thermal barrier coatings: VPS NiCoCrAlY bond coat & APS YSZ top coat**
   M. Rudolphi, D. Renusch, H.-E. Zschau and M. Schütze
   7th International Conference on the Microscopy of Oxidation, September 15 – 17, 2008, Chester, England.

5. **The role that hydrogen and sulfur play in desktop failure of thermal barrier coatings**
   M. Rudolphi, D. Renusch, H.-E. Zschau, M. Schütze, J. Meijer
   16. Jahreskolloquium des Karl-Winnacker-Instituts der DECHEMA e.V., November 27, 2008, Frankfurt am Main, Germany.
6. **The role that hydrogen and sulfur play in desktop failure of thermal barrier coatings**
   M. Rudolphi, D. Renusch, H.-E. Zschau, M. Schütze, J. Meijer
   17. Jahreskolloquium des Karl-Winnacker-Instituts der DECHEMA e.V., November 26, 2009, Frankfurt am Main, Germany.

4.2 Contributions to Conferences – Oral Presentations:

1. **Detection of Hydrogen in Hidden and Spalled Layers of Turbine Blade Coatings**, M. Rudolphi, D. Renusch, M. Schütze, J. Meijer
   36th International Conference on Metallurgical Coatings and Thin Films, April 27 – May 1, 2009, San Diego, CA, USA.
2. **Water Vapor Effects on the Spallation of Thermal Barrier Coatings**
   M. Rudolphi, D. Renusch, M. Schütze, J. L. Smialek
   2nd German Japanese Workshop on Thermal Barrier Coatings, May 27-29, 2009, Kyoto, Japan.

5 Literaturverzeichnis

[1] V. Sergo and D. R. Clarke, "Observation of Subcritical Spall Propagation of a Thermal Barrier Coating," *J. Am. Ceram. Soc.*, vol. 81, pp. 3237-3242, 1998.

[2] J. L. Smialek, "Scale Adhesion, Sulfur Content, and TBC Failure on Single Crystal Superalloys," *Ceram Eng Sci Proc.*, vol. 23, no. 4, pp. 485-495, 2002.

[3] J. G. Smeggil, "Some comments on the role of yttrium in protective oxide scale adherence," *Mater. Sci. Eng.*, vol. 87, pp. 261-265, Mar.1987.

[4] J. L. Smialek, "Effect of sulfur removal on Al2O3 scale adhesion," *Metallurgical Transactions A*, vol. 22, no. 3, pp. 739-752, 1991.

[5] J. L. Smialek, D. T. Jayne, J. C. Schaeffer, and W. H. Murphy, "Effects of hydrogen annealing, sulfur segregation and diffusion on the cyclic oxidation resistance of superalloys: a review," *Thin solid films*, vol. 253, no. 1-2, pp. 285-292, Dec.1994.

[6] B. K. Tubbs and J. L. Smialek, "Effect of sulfur removal on scale adhesion to PWA 1480," *Metallurgical and Materials Transactions A*, vol. 26, no. 2, pp. 427-435, 1995.

[7] J. L. Smialek, "The Effect of Hydrogen Annealing on the Impurity Content of Alumina-Forming Alloys," *Ox. met.*, vol. 55, no. 1/2, pp. 75-86, 2001.

[8] M.Dietrich, D.Rensuch, and M.Schütze, "The Role that Hydrogen and Sulfur Play in Desktop Failure of Thermal Barrier Coatings," *DFG Abschlussbericht*, vol. DFG-Schu 729/13-1 2005.

[9] M. Rudolphi, D. Renusch, H.-E. Zschau, and M. Schütze, "The effect of moisture on the delayed spallation of thermal barrier coatings: VPS NiCoCrAlY bond coat + APS YSZ top coat," *Materials at High Temperatures*, vol. 26, no. 3, pp. 325-329, 2009.

[10] B. R. Lawn, "An atomistic model of kinetic crack growth in brittle solids," *J. Mater. Sci.*, vol. 10, no. 3, pp. 469-480, 1975.

[11] S. M. Wiederhorn, "Moisture assisted crack growth in ceramics," *International Journal of Fracture*, vol. 4, no. 2, pp. 171-177, 1968.

[12] S. M. Wiederhorn, S. W. Freiman, E. R. Fuller Jr, and C. J. Simmons, "Effects of water and other dielectrics on crack growth," *J. Mater. Sci.*, vol. 17, no. 12, pp. 3460-3478, 1982.

[13] Z.-Y. Deng, Y.-F. Liu, Y. Tanaka, H.-W. Zhang, J. Ye, and Y. Kagawa, "Temperature Effect on Hydrogen Generation by the Reaction of gama-Al2O3-Modified Al Powder with Distilled Water," *J. Am. Ceram. Soc.*, vol. 88, no. 10, pp. 2975-2977, 2005.

[14] J. L. Smialek, "Moisture-Induced Spallation and Interfacial Hydrogen Embrittlement of Alumina Scales," NASA, 1 NASA Technical Memorandum 2005-214030, 2005.

[15] M. Yoshimura, T. Noma, K. Kawabata, and S. Somiya, "Role of H2O on the degradation process of Y-TZP," *J. Mater. Sci. Lett.*, vol. 6, no. 4, pp. 465-467, Apr.1987.

[16] D. Renusch, H. Echsler, and M. Schütze, "Life Time Modeling of APS-TBC by Using Acoustic Emission Analysis", proceedings of Turbomat Symposium 2002 (2002), pp. 48-52.

[17] D. Renusch, H. Echsler, and M. Schütze, "Progress in life time modeling of APS-TBC Part II: Critical strains, macro-cracking, and thermal fatigue," *Materials at High Temperatures*, vol. 21, no. 2, pp. 1-13, 2004.

[18] J. L. Smialek, D. Zhu, and M. D. Cuy, "Moisture-induced delamination video of an oxidized thermal barrier coating," *Scripta Materialia*, vol. 59, no. 1, pp. 67-70, 2008.

[19] M. Rudolphi, D. Renusch, and M. Schütze, "Verification of moisture-induced delayed failure of thermal barrier coatings," *Scripta Materialia*, vol. 59, no. 2, pp. 255-257, 2008.

[20] R. J. Charles, "Dynamic Fatigue of Glass," *J. Appl. Phys.*, vol. 29, no. 12, pp. 1657-1662, 1958.

[21] R. J. Charles and W. B. Hillig, "The Kinetics of Glass Failure by Stress Corrosion," in *Symposium sur la résistance mécanique du verre et les moyens de l'améliorer* Charleroi, Belgium: Union Scientifique Continentale du Verre, 1962, pp. 511-527.

Desktop Failure Map

	Experimental parameters	APS (1)	APS (2)	EB-PVD
1	Isothermal oxidation (1100°C, ~1000h, laboratory air) & water immersion at RT	No DTS observed	Not tested	DTS
2	Isothermal oxidation (1100°C, ~1000h, laboratory air) & water vapor at ~50°C	DTS	Not tested	DTS
3	Isothermal oxidation (1100°C, ~1000h, laboratory air) & dry air at RT	No DTS observed	Not tested	DTS
4	Isothermal oxidation (1100°C, 1000h, dry air) & laboratory air at RT	DTS	No DTS observed (up to 1500h)	DTS
5	Isothermal oxidation (1100°C, 1000h, humid air 10% H_2O) & laboratory air at RT	No DTS observed	No DTS observed (up to 1500h)	DTS
6	Isothermal oxidation (1100°C, 1000h, humid air 50% H_2O) & laboratory air at RT	No DTS observed	No DTS observed (up to 1500h)	DTS
7	Isothermal oxidation (1100°C, 800h, humid air 10% H_2O & 0.1% SO_2) & laboratory air at RT	Not tested	No DTS observed (up to 800h)	Not tested

dark colors indicate experiments monitored with AE

Figure 1:
Desktop failure map generated from the performed experiments.

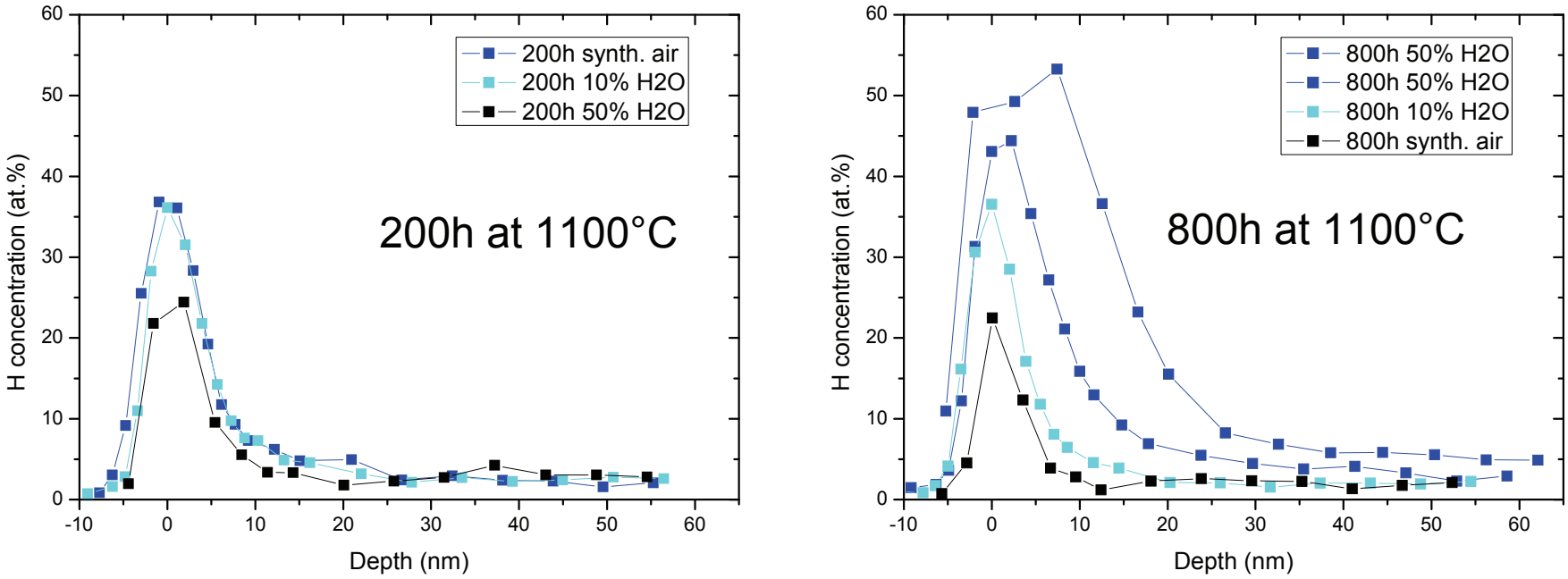

Figure 2:

Hydrogen concentration depth profiles of the TBC top surface after 200 h and 800 h oxidation, respectively, at 1100 °C in different atmospheres. While the depth profiles of the samples oxidized for 200h look rather similar, after 800 h a strong increase in H-concentration at the surface and into the YSZ coating can be observed.

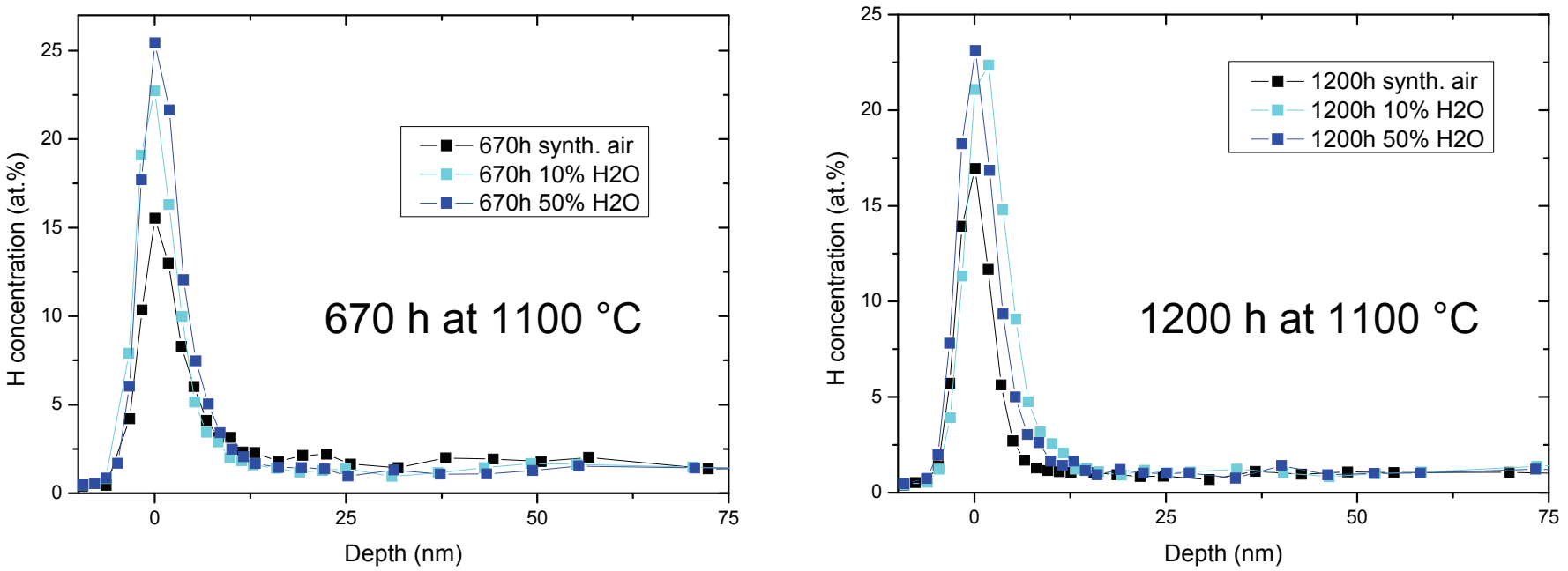

Figure 3:

Hydrogen concentration depth profiles of the exposed delamination surface after forced spallation under vacuum. Comparable amounts of hydrogen are detected which are superimposed by contamination with absorbed carbohydrates from the residual gas. Hydrogen levels from specimens oxidized in humid environment seem slightly higher.

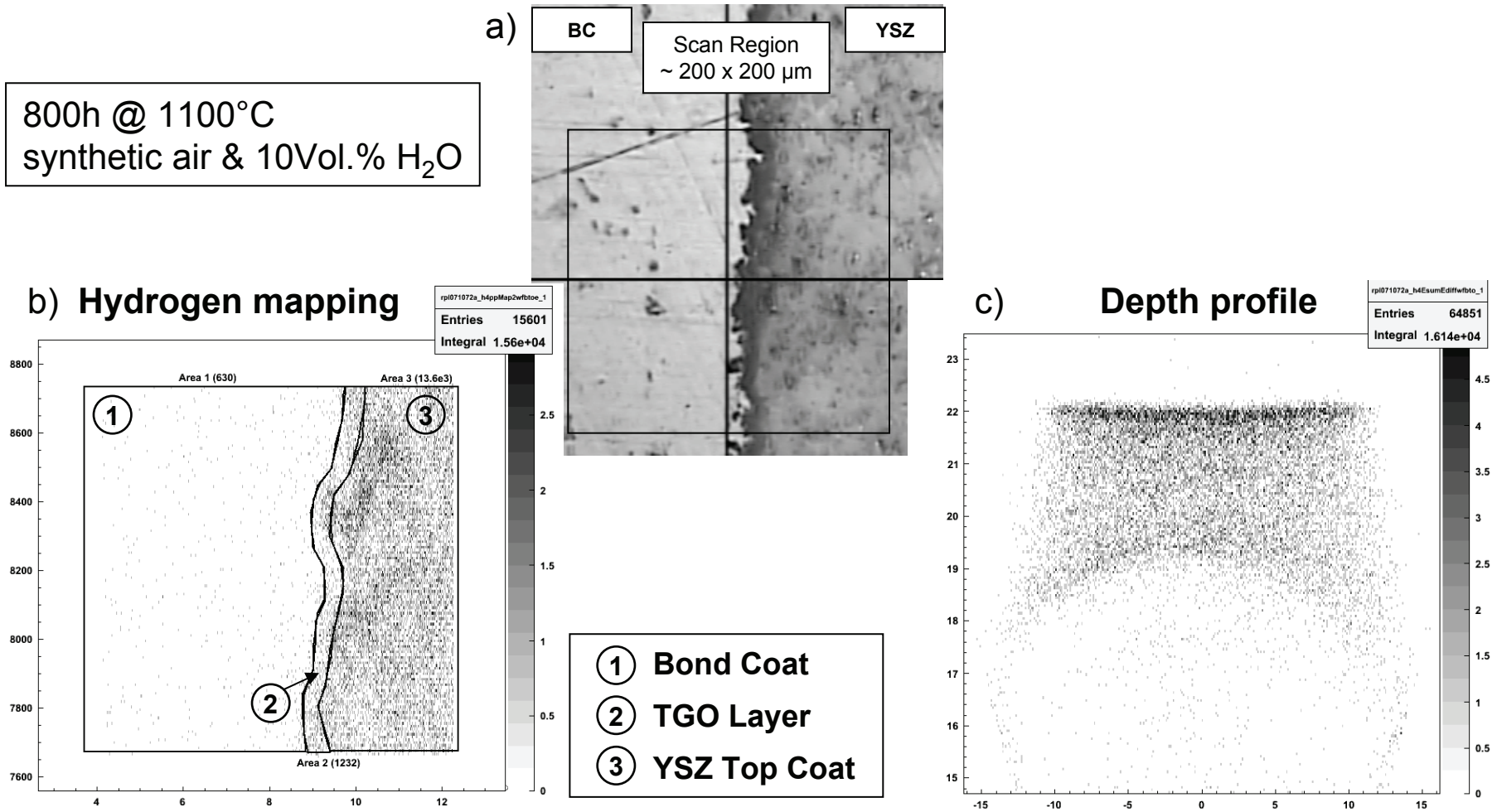

Figure 4:

Optical image of the thinned TBC cross section (a) prepared for NRA-PT measurement showing the scan region (~200 x 200 µm²). The APS(2) sample was oxidized at 1100°C for 800h in synthetic air & 10vol.% H_2O. The hydrogen mapping generated from the measurement data (b) as integral over the total thickness of cross section and hydrogen depth profile of thinned TBC cross section (c) calculated over the whole scan area. Both surfaces in the depth profile show higher hydrogen amounts (i.e. they appear darker) due to absorbed water/hydrogen, the lower surface appears bent due to proton energy loss in the sample.

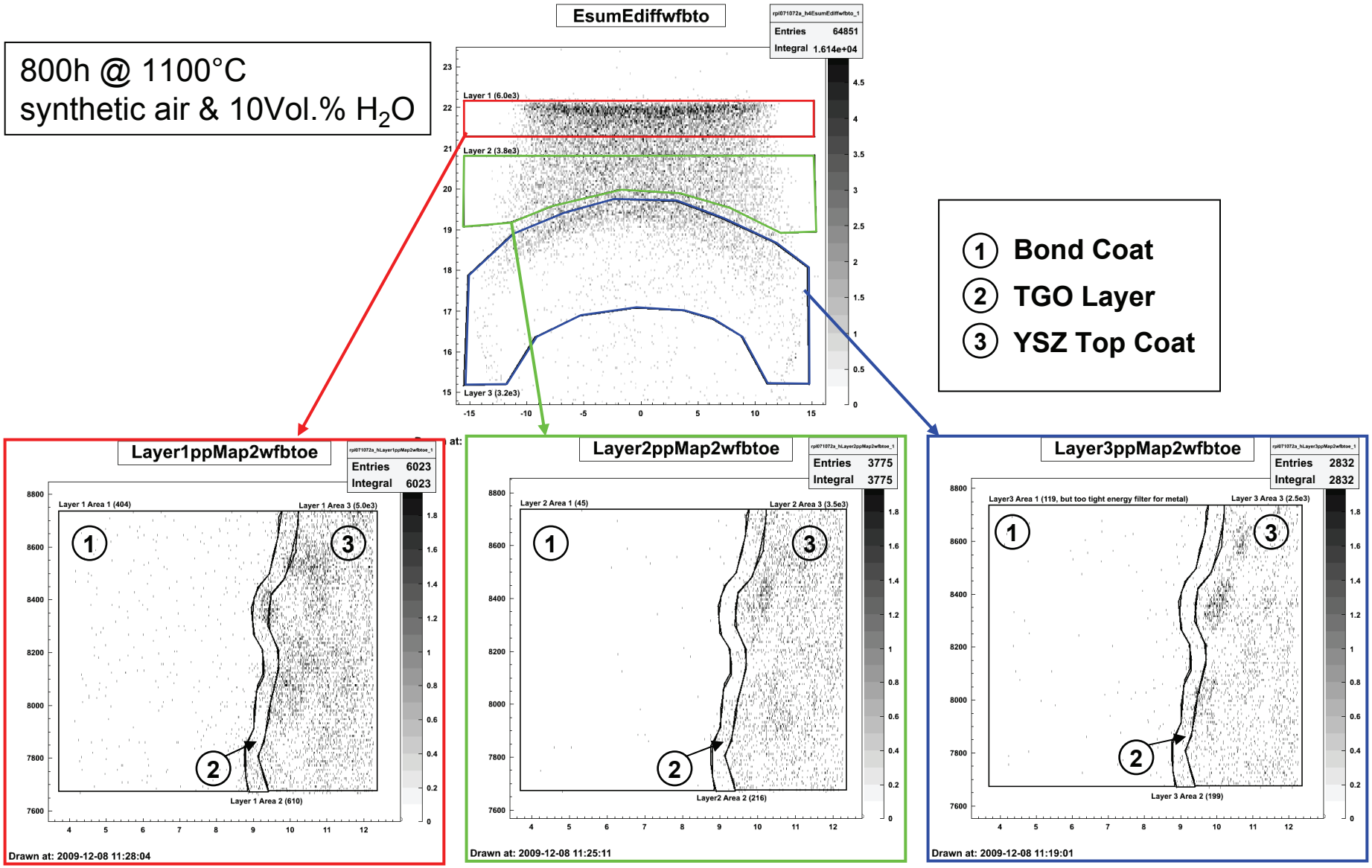

Figure 5:

Hydrogen mappings generated from different depth regions of the thinned TBC cross section. Upper surface (red) and lower surface (blue) are superimposed with absorbed water/hydrogen. A restriction to the inner volume of the cross section is given in the green mapping. Some areas show slightly increased hydrogen concentrations, however, no clear correlation with the TGO/bond coat or TGO/TBC interface can be seen. Hydrogen is almost evenly distributed within the YSZ and TGO layer.

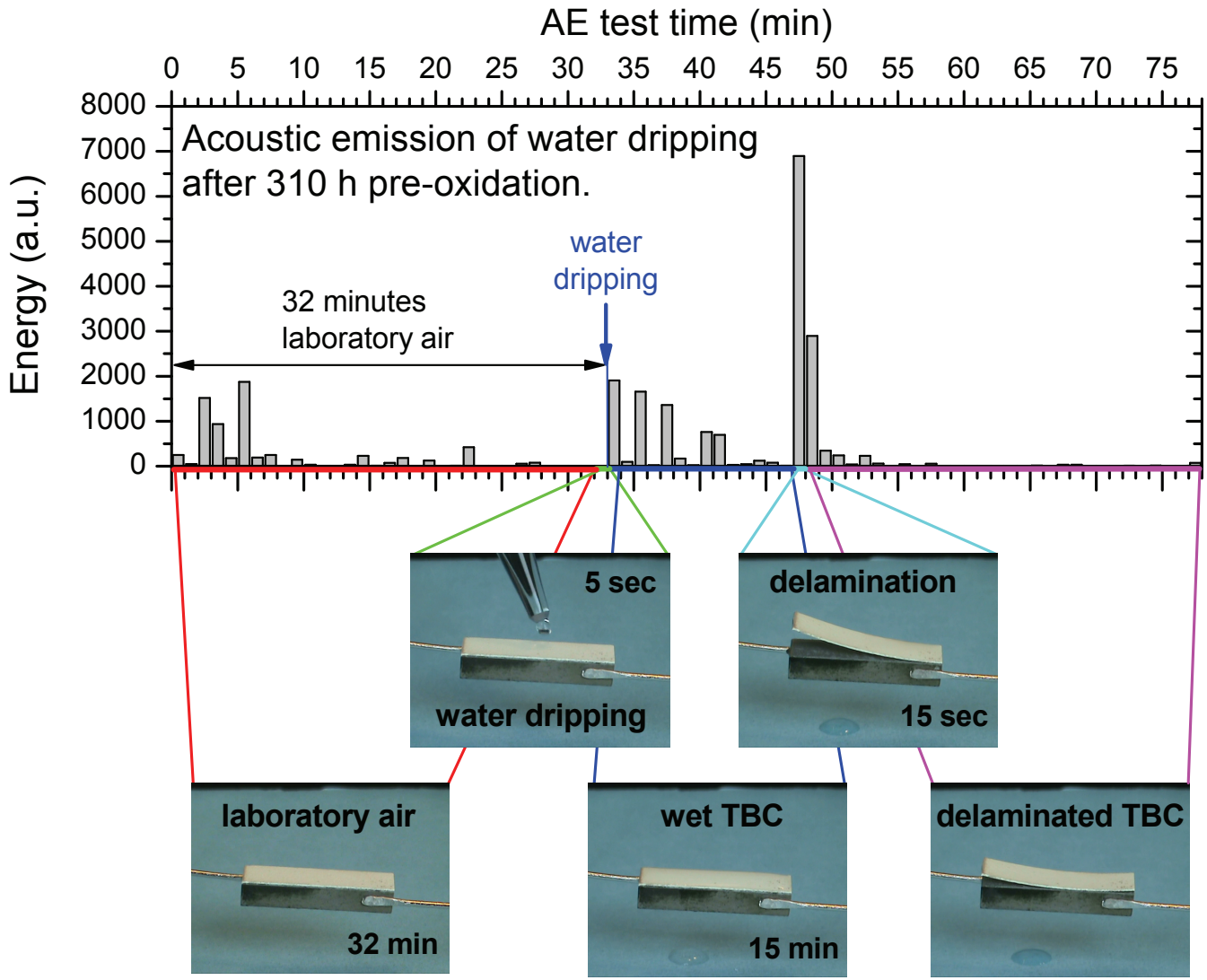

Figure 6:

Acoustic emission of 310 h pre-oxidized sample (1050 °C) and video still images from the monitor camera at certain points in time. The sample was quenched to room temperature prior to connecting the AE sensors and monitored for 32 min before water was added.

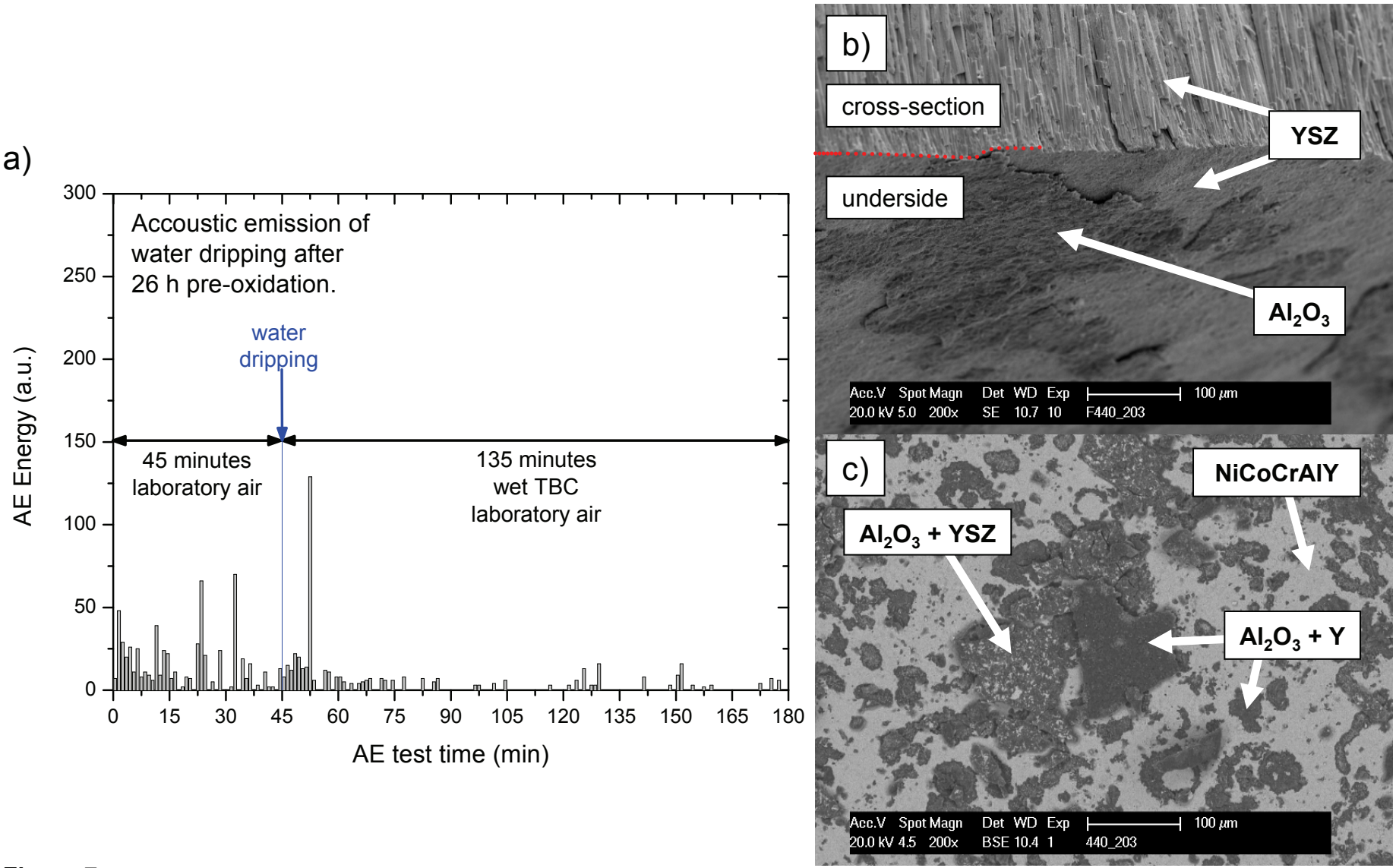

Figure 7:

Acoustic emission of EB-PVD sample pre-oxidized for 26 h at 1050 °C (a). The sample was quenched to room temperature prior to connecting the AE sensors and monitored for 45 min before water was added. No spallation was observed, however, a slight increase of acoustic emission can be seen at the time where water was dripped on the coating.

SEM micrographs taken from the sample that exhibited water induced spallation (figure 5). The delaminated TBC (b) and the delamination surface of the substrate (c) show that the failure locus is both above and below the TGO.

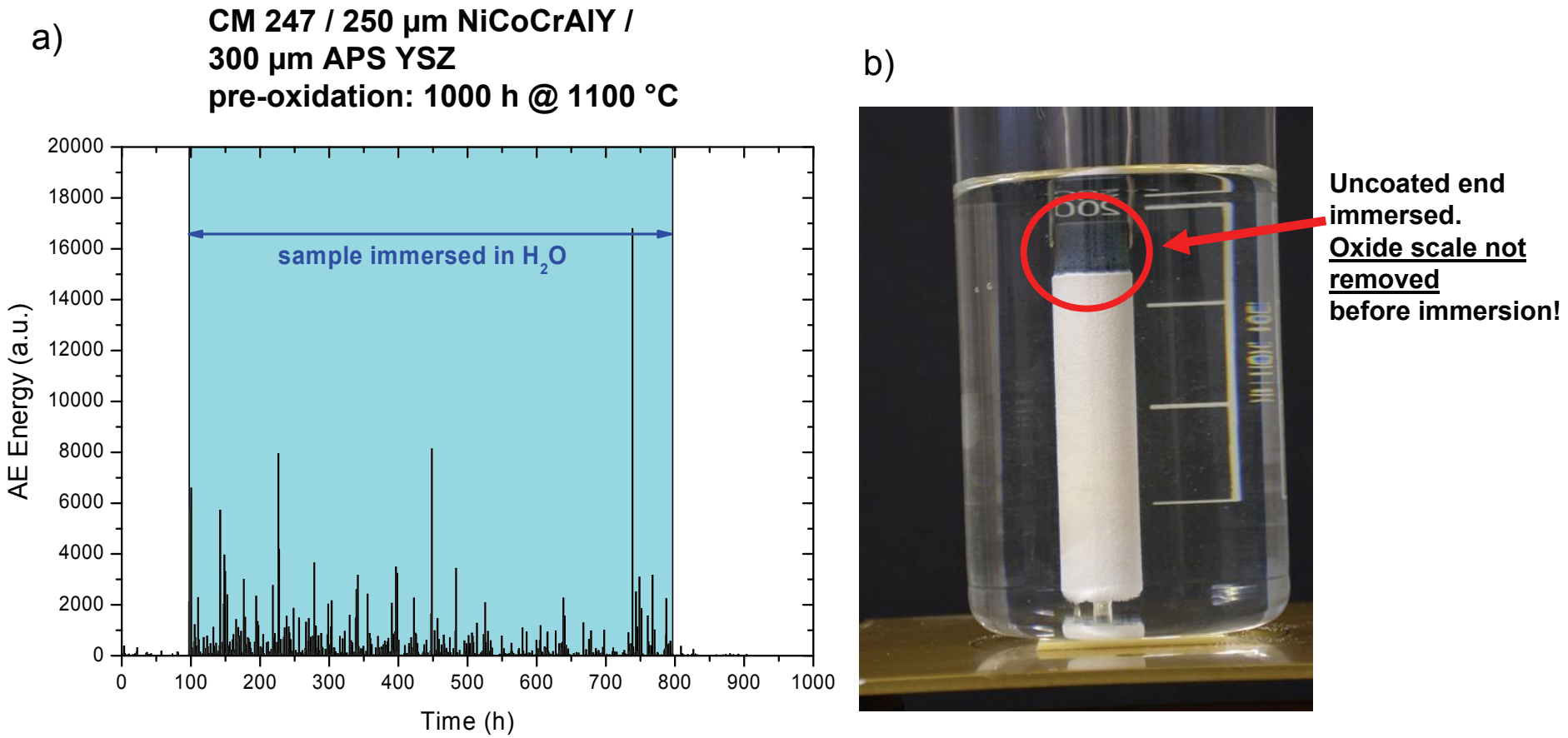

Figure 8:

Recorded acoustic emission from pre-oxidized sample (1100 °C, 1000 h, laboratory air) during water immersion (a) and photograph of the sample during immersion. The acoustic emission increased significantly upon contact of the sample with water and decreased again after the sample was removed from the water beaker. However, the uncoated part of the sample was also immersed and microcracking in the oxide scale on this part has probably contributed to the acoustic signal. Note, no macroscopic crack was observed on the sample after immersion.

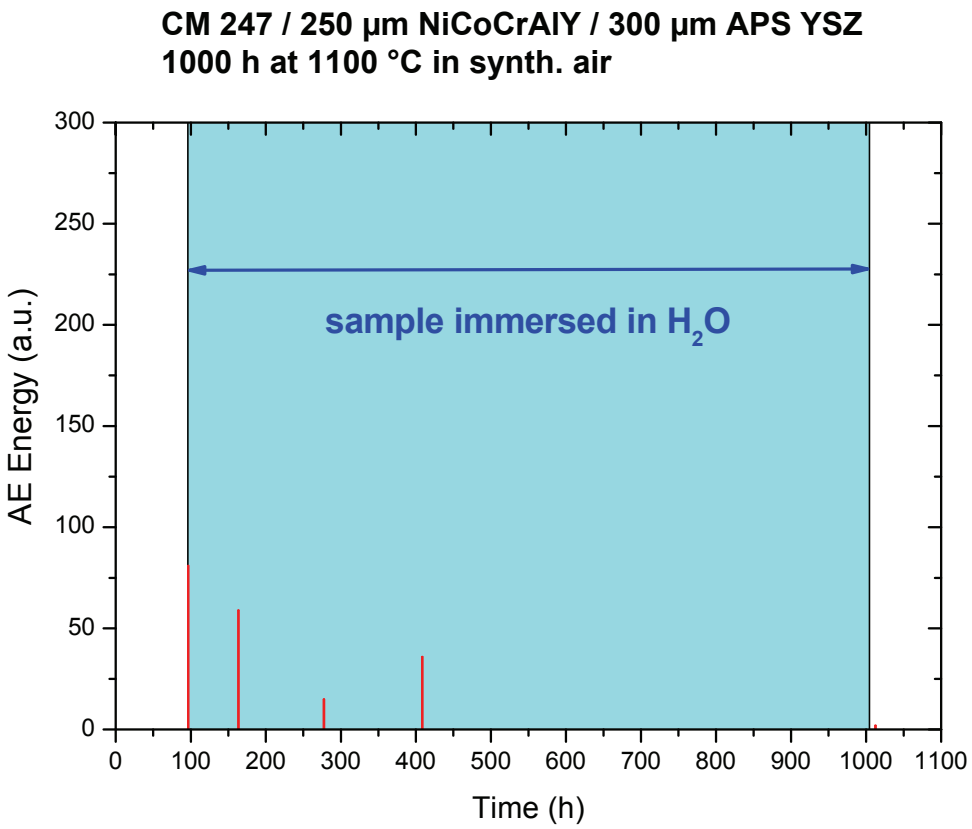

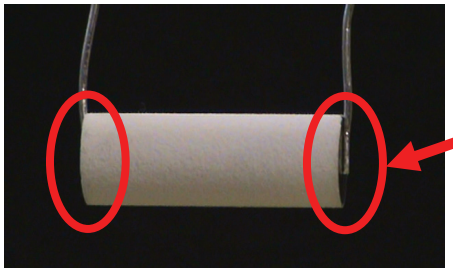

Uncoated ends immersed.
<u>Oxide scale removed</u> prior to immersion!

Figure 9:

Recorded acoustic emission from pre-oxidized sample (1100 °C, 1000 h, synthetic air) during water immersion (a) and photograph of the sample during immersion. On this sample, the uncoated ends were ground with SiC paper to remove the oxide scale prior to water immersion (see photograph (b)). Only very little acoustic emission was recorded during the test with, however, higher magnitude signals were generated during water immersion. Note, no macroscopic crack was observed on the sample after immersion.

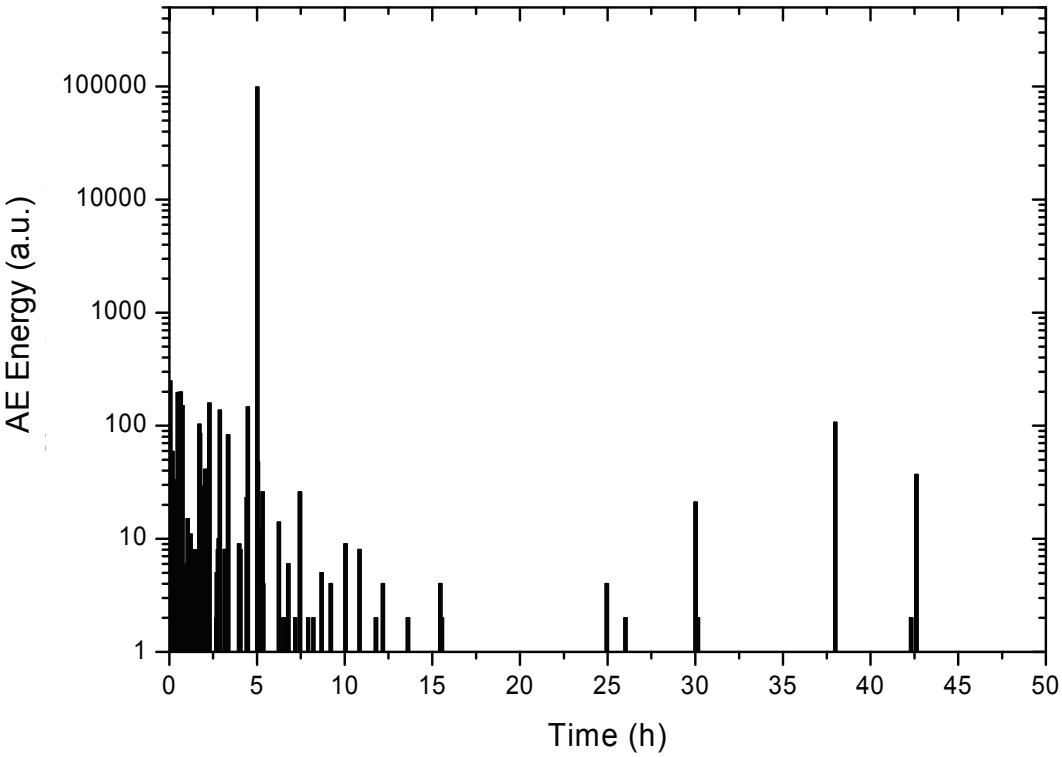

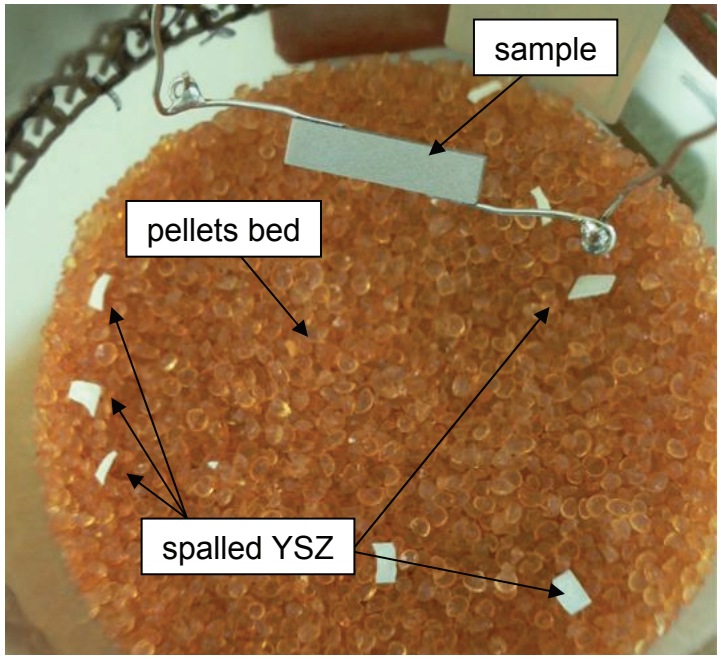

Figure 10:

Acoustic emission of 190 h pre-oxidized EB-PVD sample (1050 °C, laboratory air) and photograph of the sample after spallation. The sample was cooled from 1050 °C to room temperature within 10 minutes, then connected to acoustic emission waveguides and stored in a reactor vessel partly filled with molecular sieve pellets to create a dry environment. Nevertheless, the sample spalled over night into small pieces.

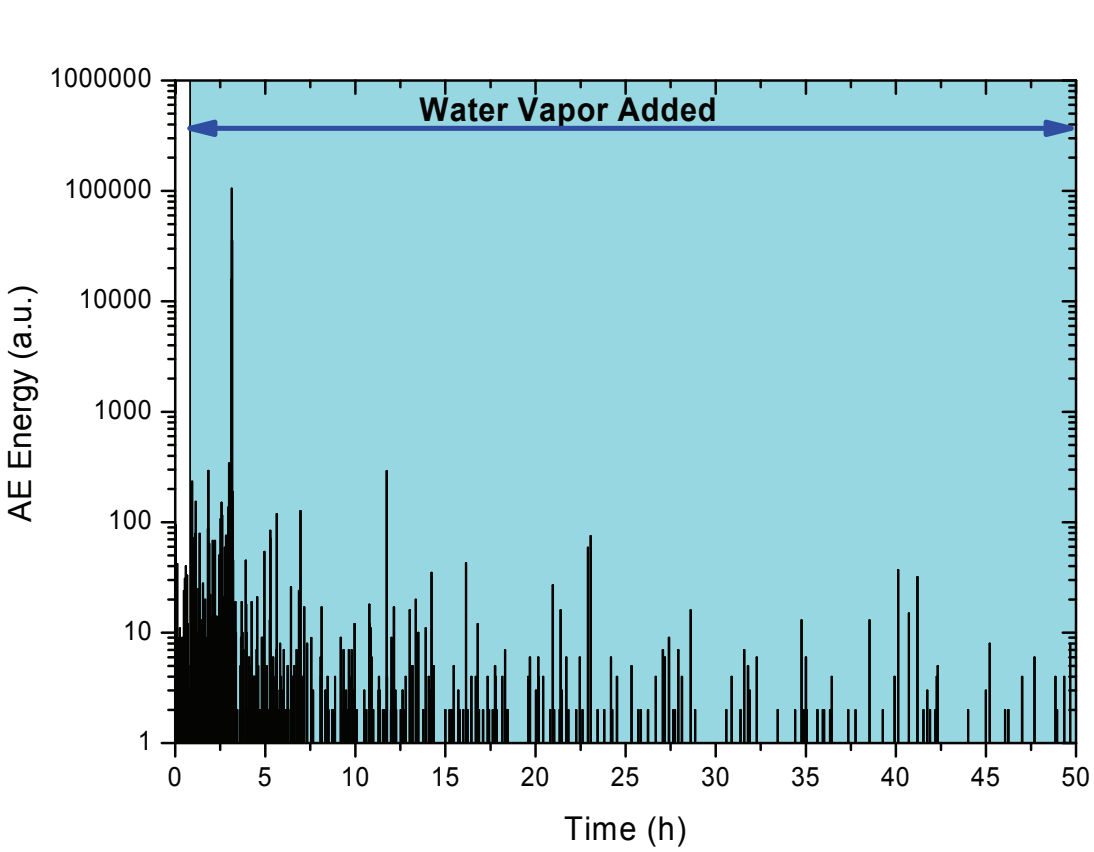

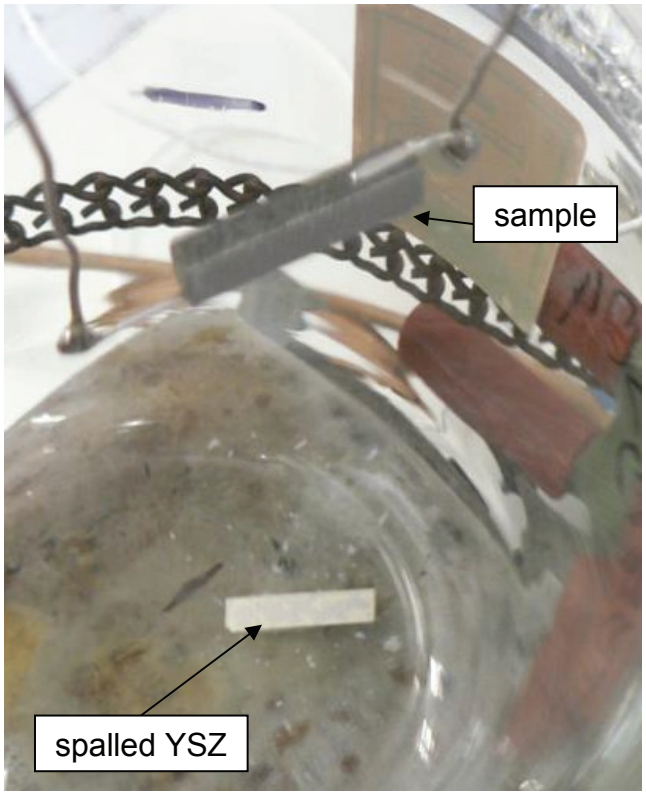

Figure 11:

Acoustic emission of 190 h pre-oxidized EB-PVD sample (1050 °C, laboratory air) and photograph of the sample after spallation. The sample was cooled from 1050 °C to room temperature within 10 minutes, then connected to acoustic emission waveguides and stored in a reactor vessel placed on a hot plate at about 50°C. Few water drops were added and the chamber was hermetically sealed to create a humidified environment. The sample spalled overnight, the YSZ top layer remained in one continuous piece.

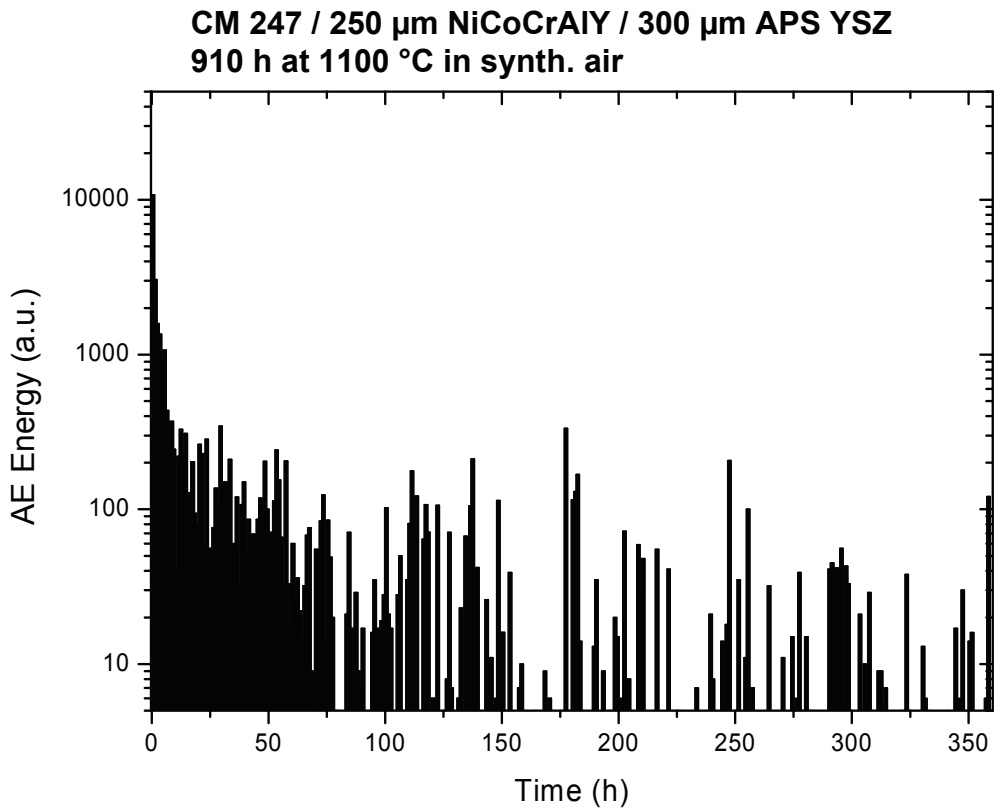

Figure 12:
Acoustic Emission signal of pre-oxidized APS sample (910 h at 1100°C) after cooling to room temperature and placing in closed reactor vessel filled with molecular sieve pellets to create a dry environment. Cooling to RT and placing in the reactor vessel took about 30 minutes. The sample remained intact for the total observation duration of 360 hours and produced significantly fewer acoustic emission than the sample stored in humid environment (see figure 9).

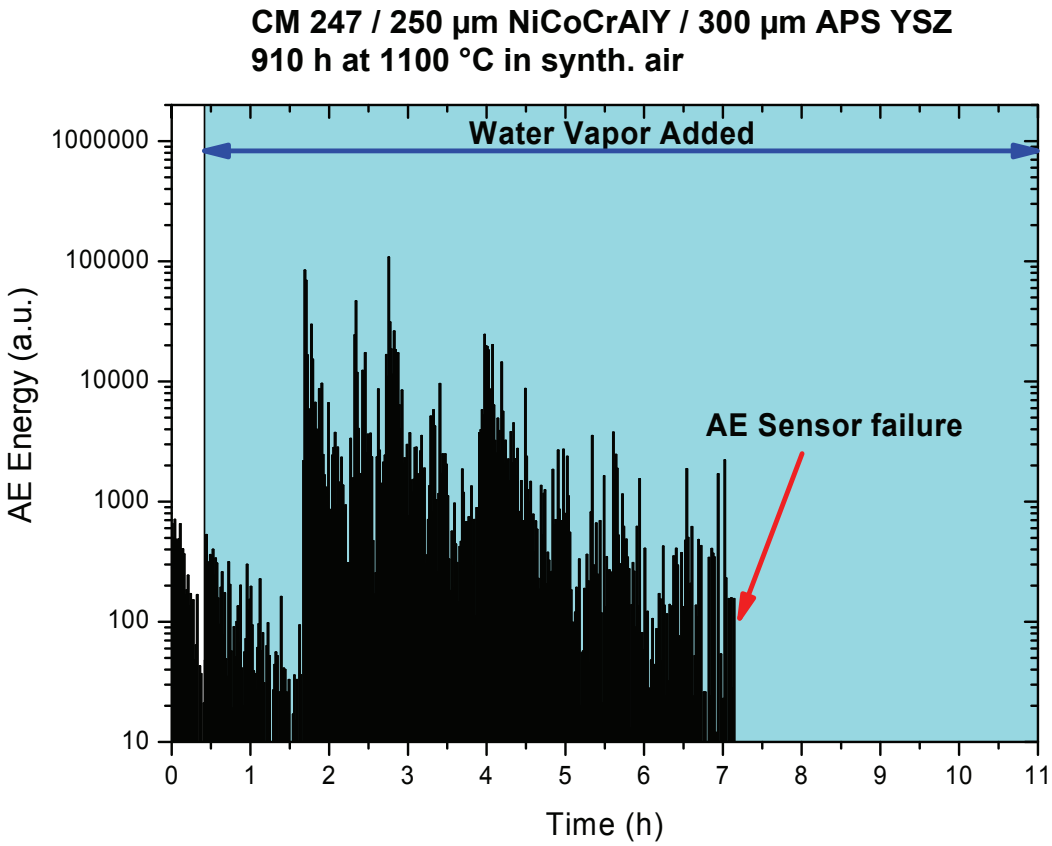

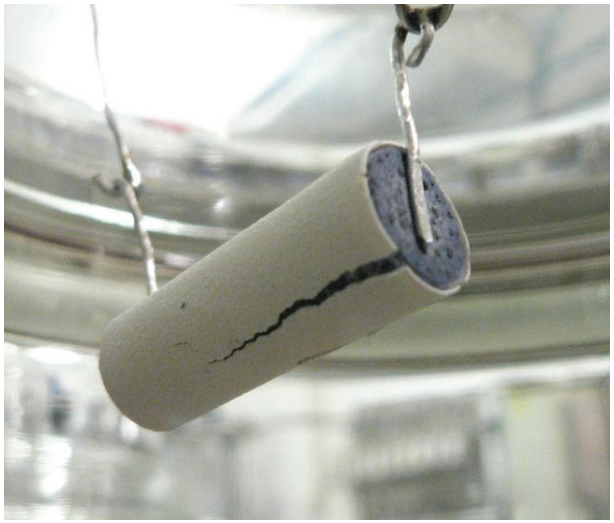

Figure 13:
Acoustic emission of 910 h pre-oxidized APS sample (1100 °C, laboratory air) and photograph of the sample after spallation. The sample was cooled from 1100 °C to room temperature within 10 minutes, then connected to acoustic emission waveguides and stored in a reactor vessel placed on a hot plate at about 50°C. Few water drops were added and the chamber was sealed hermetically to create a humidified environment. The sample spalled overnight. Note, the acoustic emission sensors failed after about 7 hours due to a PC crash.

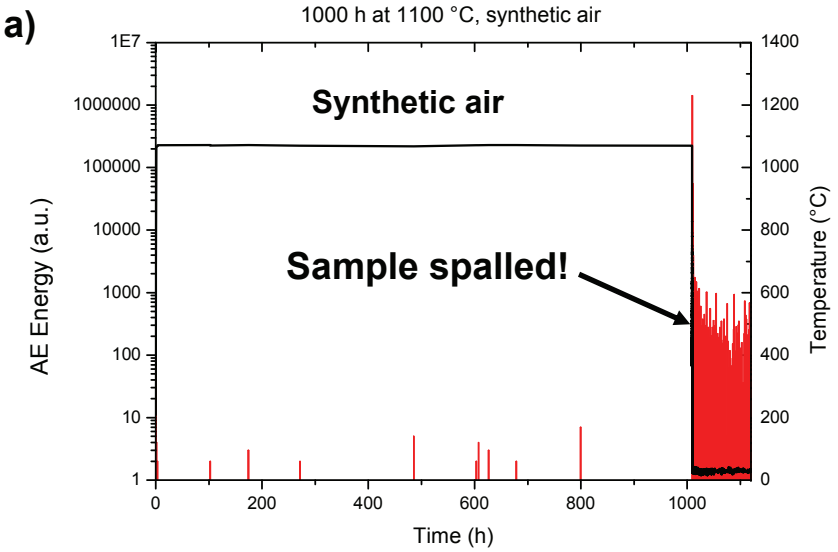

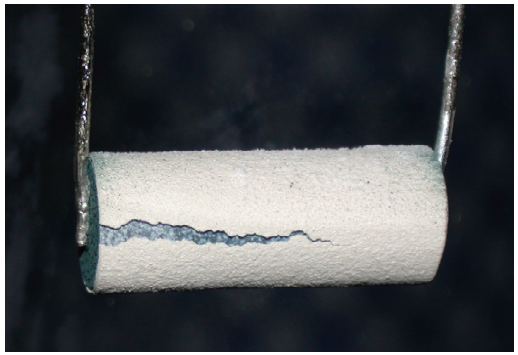

CM 247 / 250 µm NiCoCrAlY / 300 µm APS YSZ

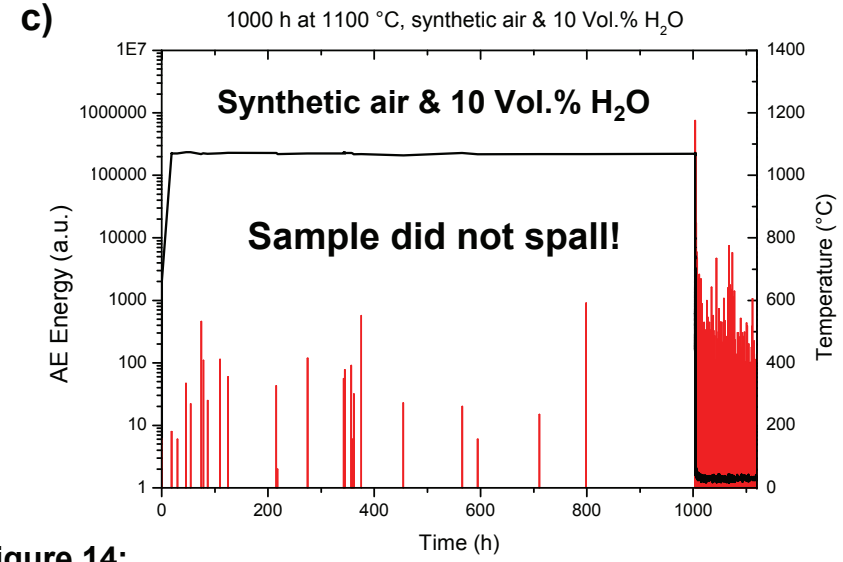

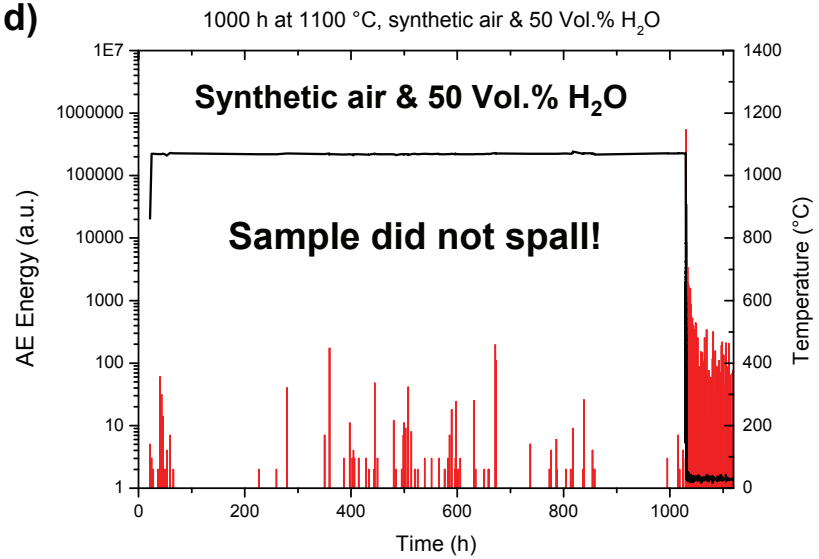

Figure 14:

Acoustic signal obtained during isothermal oxidation for 1000 h at 1100 °C in the three different atmospheres. A strong acoustic signal is observed during cooling and about 150 h after the sample is at RT – independent of the oxidizing environment. Slightly increased acoustic emission is observed during the 1000 h hot dwell at 1100 °C in the humid environments. This increase could also be caused by the unprotected sides of the cylindrical samples. The sample oxidized in dry environment spalled upon cooling, the other two samples remained intact.

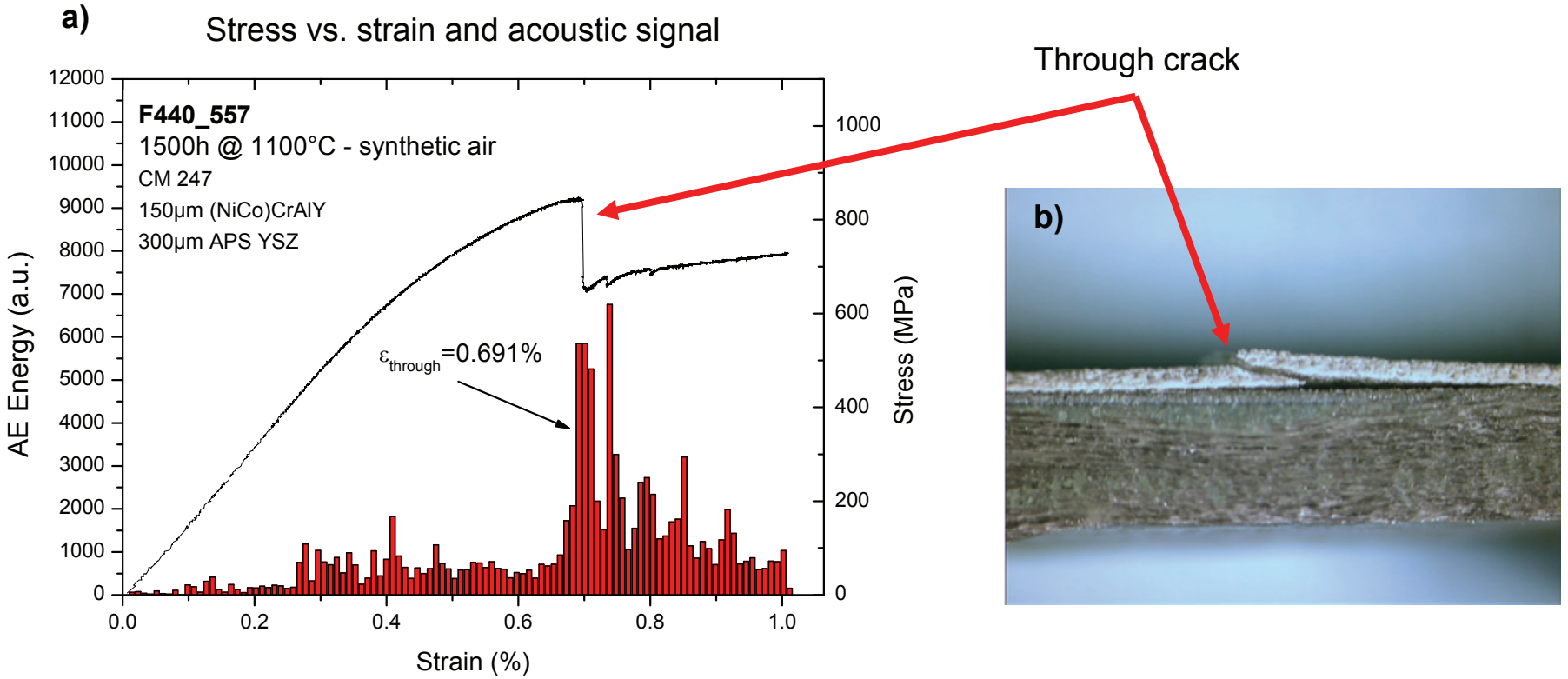

Figure 15:

Acoustic emission signal and stress/strain curve as derived from mechanical 4 point bend testing (a). The acoustic signal increases when the through-TBC crack develops and the stress drops drastically upon cracking of the TBC. Optical micrograph of TBC specimen after 4 point bend testing (b) showing through-TBC crack and partly delaminated TBC.

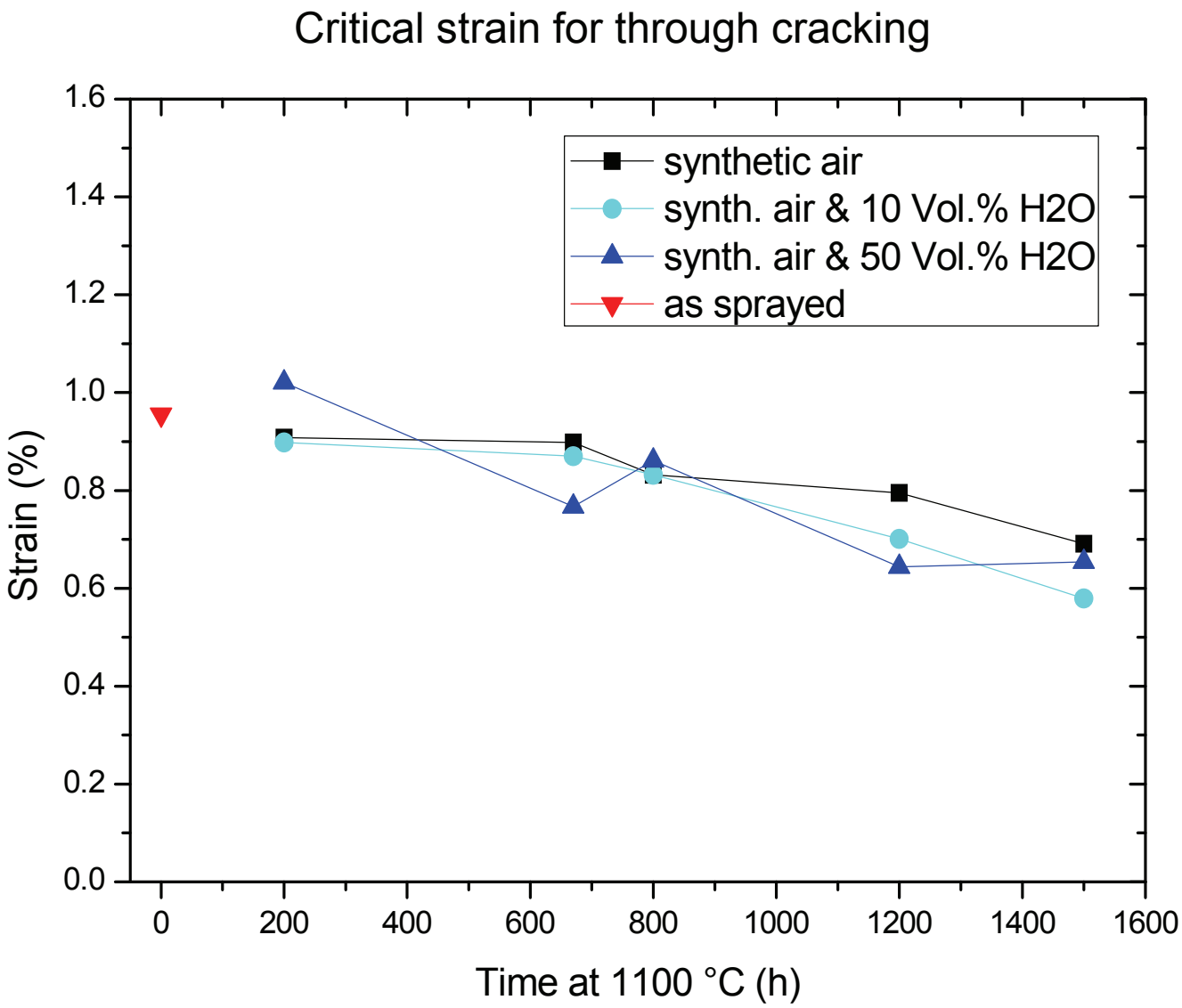

Figure 16:

Critical strain for through cracking derived from 4-pt. bend testing as a function of oxidation time at 1100 °C and oxidation environment. A slight tendency towards lower critical strain values can be observed for specimens oxidized in humid environment.

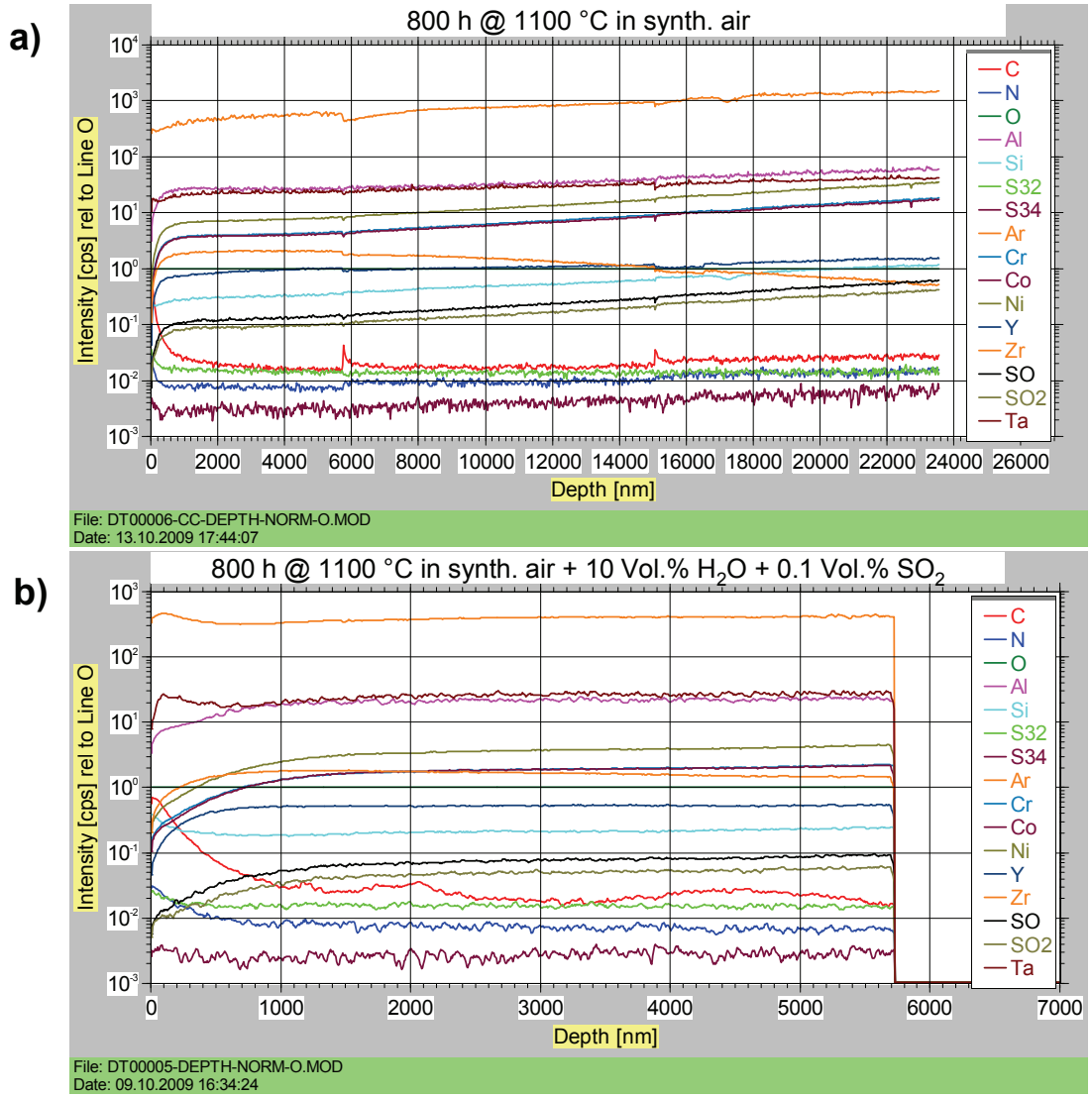

Figure 17:

SNMS concentration depth profiles of specimens oxidized for 800 h at 1100 °C in synth. air (a) and synth. air & 10 Vol.% H_2O & 0.1 Vol.% SO_2 (b). No indication of sulfur accumulation in the vicinity of the TGO can be observed neither on the ^{32}S nor on the ^{34}S lines.

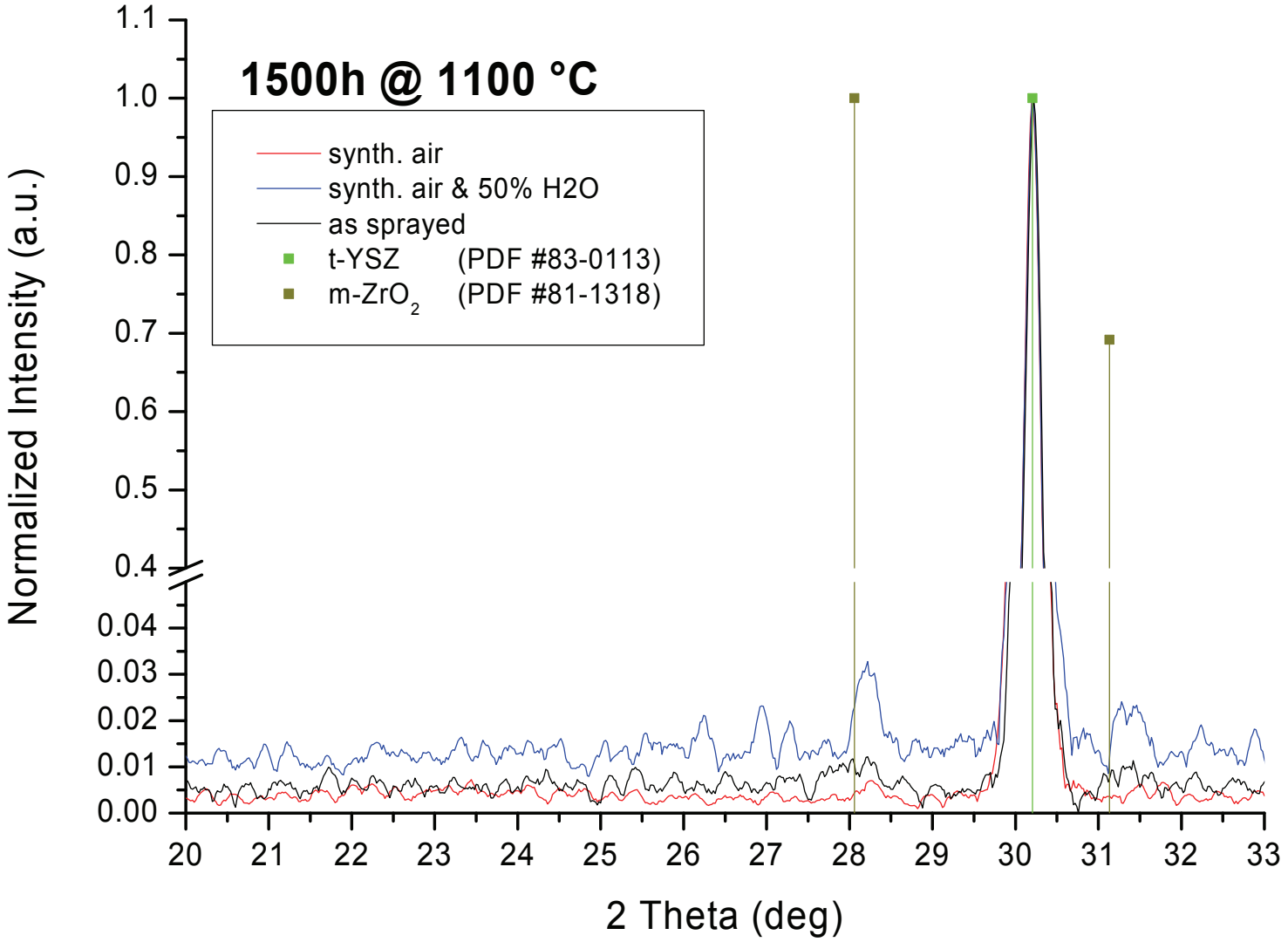

Figure 18:

XRD pattern of the top surface of oxidized APS TBC specimens in comparison with as-sprayed state. A very small fraction of monoclinic phase is present in the sample that was oxidized in humid environment, whereas the sample oxidized in dry synthetic air consists only of the tetragonal YSZ phase. Note, the sprectra were normalized with respect to the highest peak for tetragonal YSZ at 30°, the peak at 28° corresponds to the highest line in pure monoclinic ZrO_2.

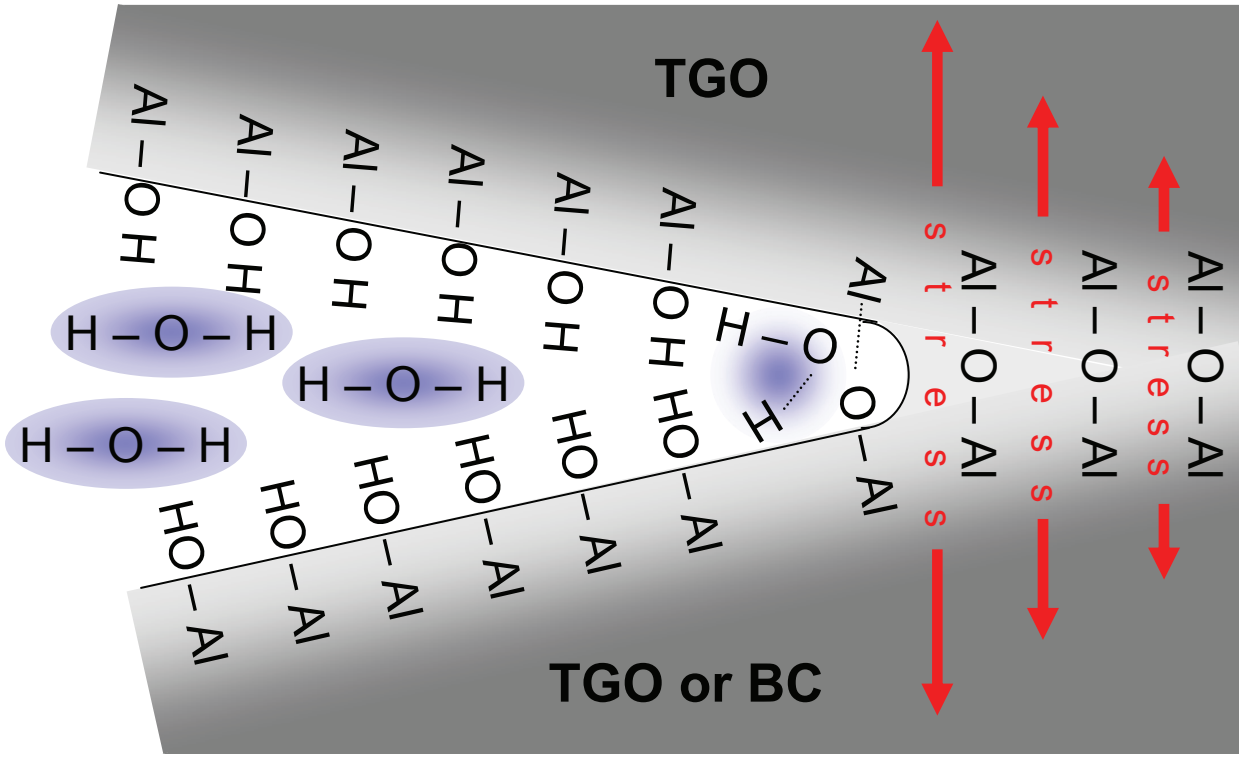

Figure 19:

Proposed mechanism for moisture induced damage and desk top spallation. Water molecules enter the crack tip (crack in either alumina or at alumina/bond coat or alumina/YSZ interface). Mechanical stresses allow access of dissociated OH^- or H^+ to oxygen bridge to form hydroxyde groups which are only weakly linked. Crack opening occurs and allows more water molecules to enter the crack tip. Crack growth can occur only as long as sufficient H_2O transport to the crack tip is ensured.

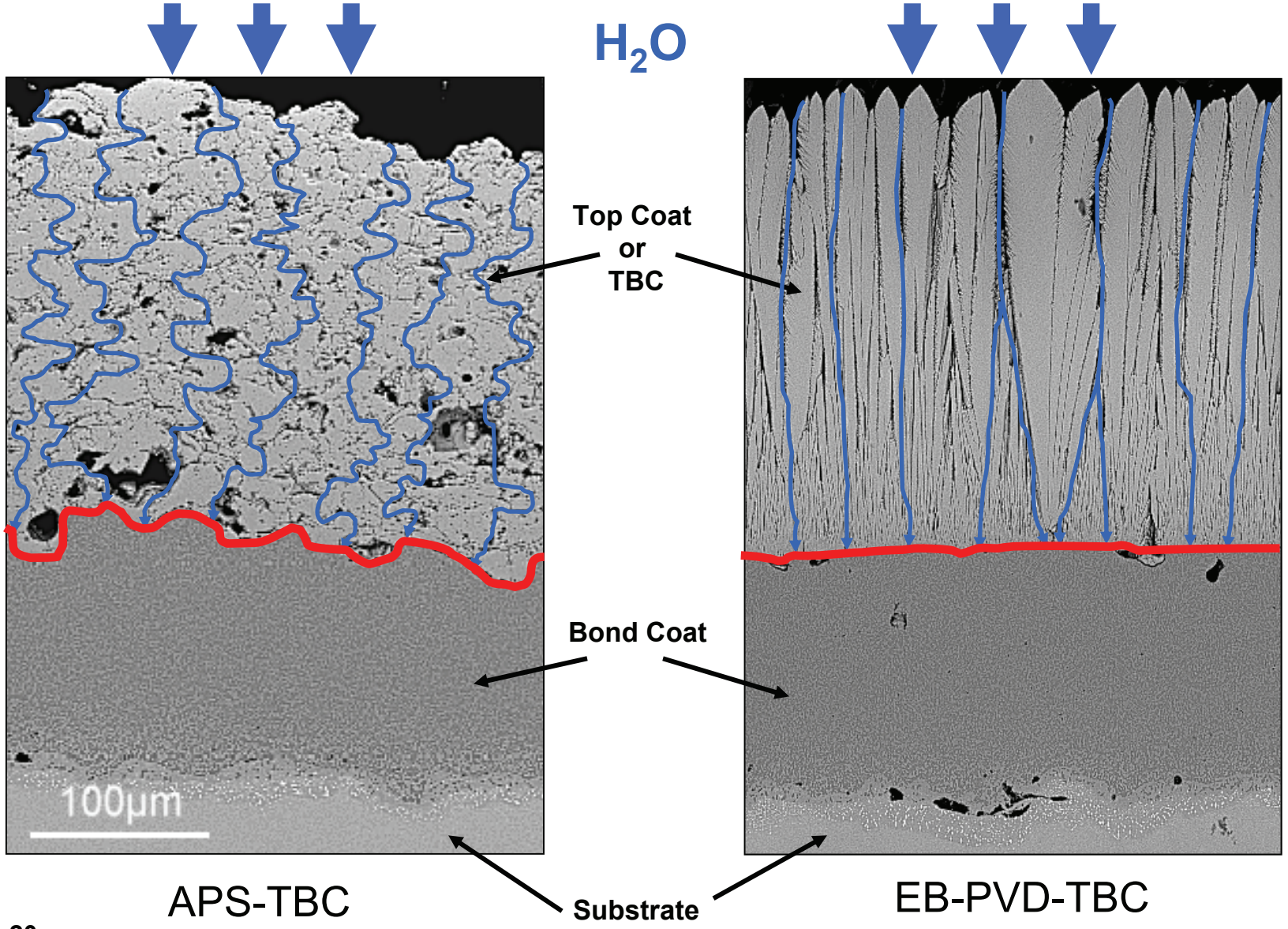

Figure 20:

Possible diffusion pathways for water (blue lines) to penetrate through the TBC to the underlying TGO layer. Clearly the columnar structure of EB-PVD allows straight-forward diffusion along intercolumnar channels whereas the APS structure enforces diffusion along zigzagging pathways provided by the splat morphology. Furthermore the flat interface morphology (red line) in EB-PVD coatings enables a fast crack growth along an almost flat plane and results in easier spallation in contrast to the rough interface of APS coatings which leads to cracks running into the bond coat or into the YSZ.